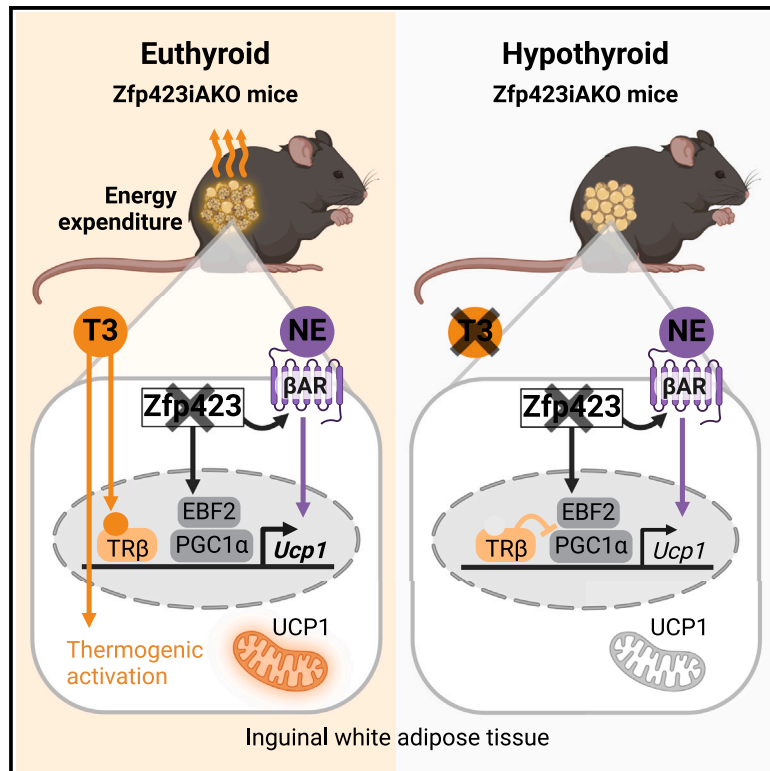


Thyroid hormones are required for thermogenesis of beige adipocytes induced by *Zfp423* inactivation

Graphical abstract



Authors

Lisa Roth, Anne Hoffmann, Tobias Hagemann, ..., Matthias Blüher, Jens Mittag, Kerstin Krause

Correspondence

kerstin.krause@medizin.uni-leipzig.de

In brief

Recruiting beige adipocytes in white adipose tissue enhances energy expenditure and improves metabolic health in mice. Roth et al. demonstrate that thyroid hormones are crucial for activating beige adipocyte thermogenesis. Their study provides insight into regulatory mechanisms that offer the potential for therapeutic targeting.

Highlights

- Thyroid hormones are crucial for UCP1-dependent thermogenesis in beige adipocytes
- Thyroid receptors (TRs) and ZFP423 cooperatively regulate the thermogenic gene program
- TRβ activation increases thermogenic activity of inguinal adipose tissue via ZFP423
- TR action correlates with expression of *ZNF423* and thermogenic genes in human adipose tissue



Article

Thyroid hormones are required for thermogenesis of beige adipocytes induced by *Zfp423* inactivation

Lisa Roth,¹ Anne Hoffmann,² Tobias Hagemann,² Leonie Wagner,¹ Christian Strehlau,² Bilal Sheikh,² Lorenz Donndorf,² Adhiteb Ghosh,³ Falko Noé,³ Christian Wolfrum,³ Knut Krohn,⁴ Juliane Weiner,¹ John T. Heiker,² Nora Klötting,² Michael Stumvoll,^{1,2} Anke Tönjes,¹ Matthias Blüher,^{1,2} Jens Mittag,⁵ and Kerstin Krause^{1,6,7,*}

¹Department of Endocrinology, Nephrology, Rheumatology, University of Leipzig Medical Center, 04103 Leipzig, Germany

²Helmholtz Institute for Metabolic, Obesity and Vascular Research (HI-MAG), Helmholtz Zentrum München, University of Leipzig and University Hospital Leipzig, 04103 Leipzig, Germany

³Institute of Food, Nutrition and Health, ETH Zurich, 8092 Zürich, Switzerland

⁴Medical Faculty, Center for DNA Technologies, University of Leipzig, 04103 Leipzig, Germany

⁵Institute of Experimental Endocrinology/CBBM, University of Lübeck, 23562 Lübeck, Germany

⁶German Center for Diabetes Research e.V., 85764 Neuherberg, Germany

⁷Lead contact

*Correspondence: kerstin.krause@medizin.uni-leipzig.de

<https://doi.org/10.1016/j.celrep.2024.114987>

SUMMARY

The significance of thyroid hormones (THs) in beige adipocyte thermogenesis remains incompletely understood. We previously reported that THs directly regulate the expression of zinc-finger protein 423 (ZFP423), an anti-thermogenic factor, in adipose tissue. This study investigates the interaction between THs and adrenergic signaling in regulating thermogenic capacity and activation of beige adipocytes formed in response to *Zfp423* deletion. We demonstrate that THs are indispensable for uncoupling protein 1 (UCP1)-dependent thermogenesis, leading to increased energy expenditure in mice with adipocyte-specific *Zfp423* knockout. Targeted activation of the thyroid receptor isoform TR β , which plays a central role in the inguinal depot, is sufficient to enhance energy expenditure in hypothyroid *Zfp423*iAKO mice. Mechanistically, THs and ZFP423 pathways cooperate to regulate early B cell factor 2 (EBF2)-mediated activation of the *Ucp1* gene. RNA sequencing (RNA-seq) analysis of human adipose tissue samples supports the relevance of this regulatory network for human adipose tissue plasticity.

INTRODUCTION

Thyroid hormones (THs) are key regulators of basal metabolic rate and adaptive thermogenesis.¹ Brown adipose tissue (BAT) is the primary site for non-shivering adaptive thermogenesis, whose activation requires the synergistic action of THs and norepinephrine (NE).² NE, which is released upon stimulation of the sympathetic nervous system (e.g., in response to cold), activates deiodinase 2 (DIO2) to increase local conversion of thyroxine (T4) to the bioactive form triiodothyronine (T3).³ Local T3 enhances β -adrenergic signaling, including β -adrenergic receptor (β AR) expression, adenylyl cyclase activity, and cyclic adenosine monophosphate (cAMP) production.^{4,5} Both T3 and cAMP cooperatively stimulate transcription of uncoupling protein 1 (UCP1), the main driver of adaptive thermogenesis in brown adipocytes.² After activation by free fatty acids released by NE-stimulated lipolysis, UCP1 disrupts the mitochondrial proton gradient. This uncouples substrate oxidation from ATP synthesis, leading to heat dissipation.^{2,6} In hypothyroidism, BAT response to cold exposure is impaired but can be restored by T4 treatment.⁷ Cold exposure or targeted β AR activation also promotes browning of classic white adipose tissue (WAT) by

the recruitment of UCP1-expressing beige adipocytes.⁸ Beige adipocytes are distinct from brown adipocytes in terms of cellular origin and molecular properties, although both have the capacity for UCP1-dependent and UCP1-independent adaptive thermogenesis.^{8,9} Interestingly, WAT browning also occurs with central or peripheral TH administration, mediated by the nuclear TH receptor isoform TR β .^{10–13}

We have shown recently in mice that TH signaling directly regulates the gene expression of zinc-finger protein 423 (ZFP423) in adipose tissue through binding of TR β to a negative TH-responsive element in the *Zfp423* promoter.¹⁴ ZFP423 is known as an early regulator of committed preadipocytes, increasing the expression of peroxisome proliferator-activated receptor γ (PPAR γ), the main driver of adipogenic differentiation.¹⁵ TH deficiency promotes the recruitment of ZFP423-expressing preadipocytes with a lipid-storing transcriptional profile.¹⁴ It has been described previously that ZFP423 maintains a white energy-storing phenotype through suppression of the thermogenic gene program.¹⁶ Accordingly, *Zfp423* expression is more abundant in white compared to brown adipocytes and is regulated in response to environmental temperature. Cold exposure and β AR activation decrease *Zfp423* expression in inguinal WAT



(iWAT), leading to morphological browning.¹⁶ Mechanistically, the transcription factor ZFP423 impedes PPAR γ occupancy and early B cell factor 2 (EBF2) co-activator recruitment to thermogenic genes.^{16,17} Additionally, ZFP423 affects UCP1-independent thermogenic pathways, such as futile creatine cycling.¹⁸ Overall, ZFP423 appears to be a promising candidate linking THs and adrenergic signaling for adaptive thermogenesis in beige adipocytes. We used mice with inducible deletion of *Zfp423* in mature white adipocytes as a suitable model to study beige thermogenesis, as described previously.^{16,18}

In this study, we addressed two questions. First, is TH-induced WAT browning driven by TR β -mediated effects on ZFP423? Second, how do THs interact with adrenergic signaling to modulate UCP1-dependent thermogenic capacity and activation of *Zfp423*-ablated beige adipocytes? Collectively, this study provides insights into the TH-driven regulatory networks governing adipocyte plasticity and their potential implications for metabolic homeostasis and energy expenditure.

RESULTS

Intact thyroid hormone signaling augments the thermogenic phenotype of *Zfp423*-ablated adipocytes in iWAT

The transcription factor ZFP423 plays an important role in the regulatory network controlling adipocyte formation and function. ZFP423 promotes the white adipocyte phenotype by suppressing the thermogenic gene program. Consequently, deletion of *Zfp423* in adiponectin-expressing cells induces a white-to-beige lineage conversion.¹⁶ We have reported previously that TH deficiency transcriptionally upregulates *Zfp423* gene expression, associated with the recruitment of preadipocytes with a lipid-storing transcriptional profile.¹⁴ Given that THs are mandatory for full adaptive thermogenesis in BAT, we aimed to examine the functional relationship between TH signaling and ZFP423 in modulating the thermogenic capacity of beige adipocytes. To this end, we generated mice with an inducible knockout of *Zfp423* in mature white adipocytes (designated *Zfp423iAKO*) by crossing mice with floxed *Zfp423* alleles¹⁹ with mice carrying a tamoxifen-inducible Cre-ER^{T2} gene under the control of the adiponectin promoter (Adipoq_CreER^{T2}).²⁰ To induce hypothyroidism (i.e., systemic TH deficiency), 8-week-old female mice were fed an iodine-free chow diet supplemented with 0.15% propylthiouracil (PTU), while euthyroid mice were maintained on a regular chow diet (Figure 1A). After 4 weeks of diet, hypothyroid (HO) mice showed significantly decreased serum levels of total T4 and free T3 and increased mRNA levels of the pituitary thyroid-stimulating hormone TSH β compared to euthyroid (EU) mice (Figures S1A and S1B). During the second week of PTU treatment, *Zfp423* knockout was induced by injecting 1 mg tamoxifen per day for 5 consecutive days. Since tamoxifen itself can induce WAT browning,²¹ it was administered to all mice, including the controls that carried no Cre transgene but floxed *Zfp423* alleles (Figure 1A). Weight gain in mice receiving the PTU diet was attenuated by tamoxifen treatment but increased again 1 week after the last injection (Figure 1B). At sacrifice, there was no significant difference in body weight between the experimental groups (Figure S1C). Consistent with our previous

findings,¹⁴ *Zfp423* mRNA expression in iWAT and gonadal WAT (gWAT) was significantly higher in hypothyroid controls compared to euthyroid controls (Figure 1C). Deletion of *Zfp423* in mature white adipocytes significantly reduced *Zfp423* mRNA in iWAT and gWAT to comparable levels in eu- and hypothyroid *Zfp423iAKO* mice (Figure 1C). This was accompanied by a significant increase in total UCP1 protein (Figures 1D and S1D), UCP1-expressing adipocytes (Figures 1H and S1E), and thermogenic marker gene expression (Figures 1I and S1F) compared to controls. Notably, all features of browning induced by *Zfp423* deletion were suppressed in the iWAT depot in the absence of THs (Figures 1D, 1E, 1H, and 1I). In gWAT, there was no clear alteration in response to TH status (Figures 1F, S1E, and S1F). Calculation of the amount of UCP1 per adipose tissue depot suggests that iWAT has a markedly higher thermogenic potential than gWAT. In euthyroid *Zfp423iAKO* mice, the UCP1 amount in iWAT was even comparable to BAT (Figure 1G). In contrast to the doxycycline-inducible *Zfp423iAKO* model,¹⁶ tamoxifen-inducible Cre recombinase in our model was also effective in BAT, leading to significantly reduced *Zfp423* mRNA levels compared to control mice (Figure 1C). However, deletion of *Zfp423* in BAT had no effect on UCP1 protein expression (Figures 1D and 1G), thermogenic marker gene expression (Figure S1G), or BAT temperature (Figure 1J). Overall, the data show that TH signaling augments the thermogenic program in *Zfp423*-ablated beige adipocytes of the iWAT depot but not the gWAT depot.

Thyroid hormones are indispensable for thermogenic activation of *Zfp423*-ablated beige adipocytes

The synergistic action of thyroid and adrenergic hormones for adaptive thermogenesis in BAT is well established, but its role in beige adipocytes is not fully clear. Therefore, we next investigated the interaction between THs and adrenergic signaling on thermogenic capacity of beige adipose tissue in *Zfp423iAKO* mice. To this end, *Zfp423iAKO* mice and littermate controls were housed at 30°C (thermoneutrality), 22°C (room temperature), and 18°C (cold stress) throughout the 4 weeks of PTU-containing diet or chow diet (Figure 2A). Instead of 4°C, a cold stress of 18°C was chosen, since it allows to study the recruitment of adaptive thermogenesis in hypothyroid mice, which would die of hypothermia at lower temperatures.²² UCP1 protein expression in iWAT of hypothyroid controls was absent regardless of ambient housing temperature. However, the deletion of *Zfp423* in hypothyroid mice resulted in detectable UCP1 protein expression already at thermoneutrality, indicating that *Zfp423* deletion alone is sufficient to induce UCP1 expression in iWAT even in the absence of intact TH and NE signaling (Figures 2B and S2A). The amount of UCP1 was amplified by both the presence of TH and in response to decreasing ambient temperature (Figure 2B). Next, we examined whether increased UCP1 expression translated into thermogenic activity and higher energy expenditure. Whole energy expenditure measured by indirect calorimetry was increased exclusively in euthyroid *Zfp423iAKO* mice compared to euthyroid controls ($p = 0.0011$), while *Zfp423* deletion failed to stimulate energy expenditure in hypothyroid mice irrespective of ambient temperature ($p = 0.9995$) (Figures 2C, S2B, and S2C). It suggests that TH signaling is mandatory to fully activate the thermogenic function of beige adipocytes formed in

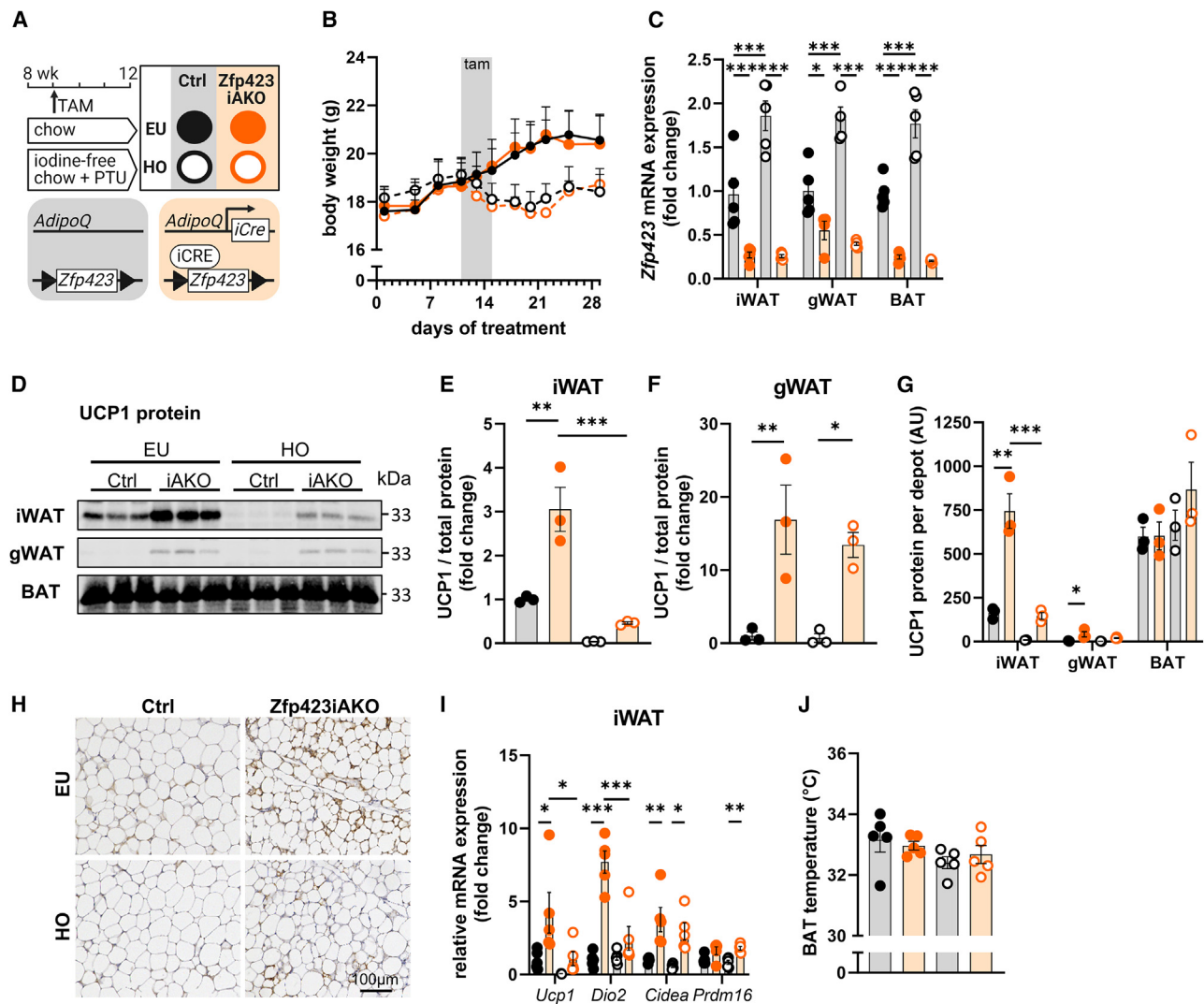


Figure 1. Intact thyroid hormone signaling augments the thermogenic phenotype of *Zfp423*-ablated adipocytes in iWAT

(A) Female *Zfp423*iAKO mice and floxed littermate controls (Ctrl) were treated with tamoxifen (1 mg intraperitoneally [i.p.], 5 days) to induce adipocyte-specific *Zfp423* deletion. Mice were rendered euthyroid (EU) and hypothyroid (HO) by feeding a chow diet or iodine-free chow diet complemented with 0.15% PTU for 4 weeks, respectively.

(B) Body weight progress during treatment. $n = 5$.

(C) *Zfp423* mRNA expression in inguinal white adipose tissue (iWAT), gonadal WAT (gWAT), and brown adipose tissue (BAT) of eu- and hypothyroid *Zfp423*iAKO and control mice, represented as fold change to the Ctrl/EU group. $n = 4-5$.

(D) Western blot of UCP1 protein expression in iWAT, gWAT, and BAT. $n = 3$.

(E and F) Relative UCP1 protein expression in (E) iWAT and (F) gWAT, represented as fold change to the Ctrl/EU group. $n = 3$. Signal intensity was normalized to total protein (Figure S1D).

(G) Total UCP1 protein amounts per adipose tissue depot. $n = 3$.

(H) Immunohistochemical staining of UCP1 in iWAT sections. Representative images, $n = 3$.

(I) mRNA expression of thermogenic genes in iWAT, such as *Ucp1*, *Dio2*, *Cidea*, and PR domain containing 16 (*Prdm16*), represented as fold change to the Ctrl/EU group. $n = 5$.

(J) BAT temperature calculated from infrared thermography. $n = 5$.

Data are represented as mean \pm SEM. Two-way ANOVA with Tukey post hoc test for multiple comparisons. * $p < 0.05$, ** $p < 0.01$, *** $p < 0.001$. See also Figure S1.

response to *Zfp423* deletion (interaction $p = 0.009$; Table S1). Consistent with this notion, the increased energy expenditure in euthyroid *Zfp423*iAKO mice was associated with stabilized body temperature at 18°C, while body temperature dropped in

control mice in response to this cold stress (Figure 2D). Since BAT is the major site of adaptive thermogenesis in mice, we wanted to confirm that *Zfp423* deletion in WAT but not in BAT elicited whole-body energy expenditure. Therefore, we

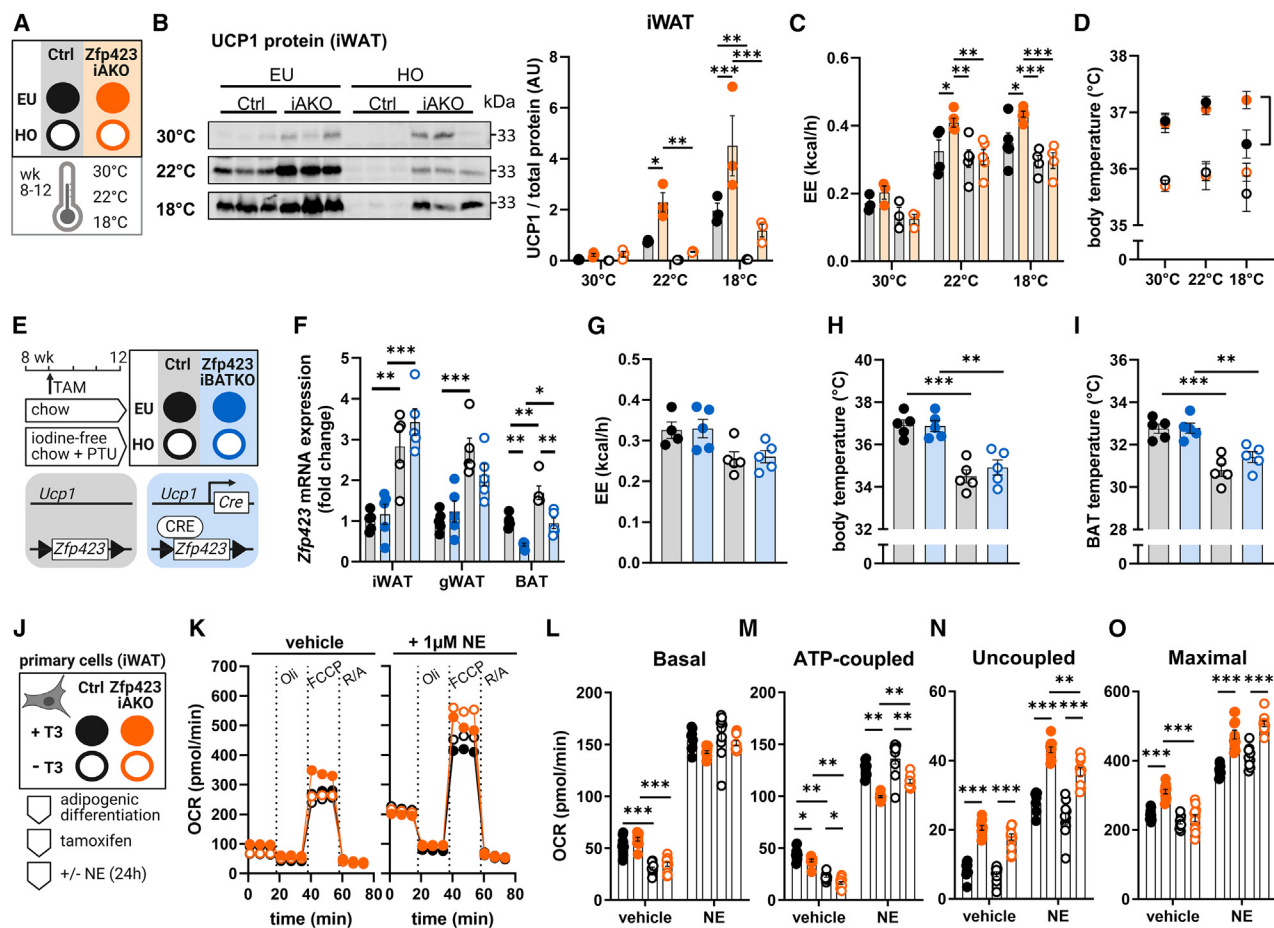


Figure 2. Thyroid hormones are indispensable for thermogenic activation of *Zfp423*-ablated beige adipocytes

(A) Female *Zfp423*iAKO mice and floxed littermate controls (Ctrl) were rendered euthyroid (EU) and hypothyroid (HO) and treated with tamoxifen as described in Figure 1A. During the 4 weeks of treatment, mice were held at 30°C, 22°C, or 18°C.

(B) Western blot of UCP1 protein expression in iWAT of mice at different housing temperatures. $n = 3$. Signal intensity was normalized to total protein (Figure S2A). Data for 22°C are the same as for Figure 1D.

(C) Mean energy expenditure. $n = 3$ (30°C), $n = 4-5$ (22°C, 18°C). See Figures S2B and S2C and Table S1 for statistical analysis.

(D) Body temperature at the end of treatment. $n = 4-5$.

(E) Female *Zfp423*iBATKO mice and floxed littermate controls (Ctrl) were treated with tamoxifen for 5 days to induce *Zfp423* deletion in UCP1-expressing adipocytes and were rendered eu- and hypothyroid as described before.

(F) *Zfp423* mRNA expression in iWAT, gWAT, and BAT, represented as fold change to the Ctrl/EU group. $n = 5$.

(G) Mean energy expenditure. $n = 4-5$. See Figure S2D and Table S2 for statistical analysis.

(H and I) Body temperature (H) and BAT temperature (I) calculated from infrared thermography. $n = 5$.

(J) Stromal vascular cells isolated from iWAT of *Zfp423*iAKO and control mice were differentiated in TH-depleted medium with or without 10 nM T3. *Zfp423* deletion was induced by treatment with 1 μM tamoxifen for 48 h, followed by 48 h of washout and stimulation with 1 μM NE or vehicle for 24 h.

(K) Oxygen consumption rate (OCR) progress after stimulation with 2 μM oligomycin (Oli), 2.5 μM FCCP (CAS: 370-86-5), and 0.5 μM rotenone/antimycin A (R/A). Three mice per genotype (Ctrl/*Zfp423*iAKO) were pooled and measured in technical replicates. $n = 8-12$.

(L) Basal respiration calculated as (basal OCR) – (minimal OCR after R/A).

(M) ATP-coupled respiration calculated as (basal OCR) – (minimal OCR after Oli).

(N) Uncoupled respiration calculated as (minimal OCR after Oli) – (minimal OCR after R/A).

(O) Maximal respiration calculated as (maximal OCR after FCCP) – (minimal OCR after R/A).

Data are represented as mean ± SEM. Two-way ANOVA with Tukey post hoc test for multiple comparisons. * $p < 0.05$, ** $p < 0.01$, *** $p < 0.001$. See also Figure S2 and Tables S1 and S2.

crossed *Zfp423*-floxed mice with UCP1_{CreERT2} mice to delete *Zfp423* only in UCP1-expressing adipocytes (designated *Zfp423*iBATKO; Figure 2E). *Zfp423* expression was unaffected in iWAT and gWAT of *Zfp423*iBATKO mice compared to controls, whereas it was reduced in BAT (Figure 2F). There was no differ-

ence in energy expenditure, body temperature, or BAT temperature between euthyroid *Zfp423*iBATKO mice and euthyroid controls (Figures 2G–2I and S2D; Table S2). Together, these data confirm that *ZFP423* specifically modulates the thermogenic capacity of white adipocytes but not of brown adipocytes. To further

investigate the distinct effects of THs and NE on thermogenic activation of beige adipocytes, we measured mitochondrial oxygen consumption rate (OCR) on a cellular level. To this end, stromal vascular cells were isolated from iWAT of *Zfp423iAKO* and control mice and differentiated in TH-depleted medium in the presence or absence of 10 nM T3 to mimic the euthyroid or hypothyroid status, respectively (Figure 2J). *Zfp423* knockdown was efficiently induced by tamoxifen treatment in the differentiated adipocytes (Figure S2E), and the OCR was measured after stimulation with 1 μ M NE or vehicle for 24 h (Figures 2J and 2K). In the absence of adrenergic stimulation, a higher basal OCR was detected in T3-treated adipocytes (Figure 2L), mainly attributed to increased ATP-coupled respiration (oligomycin blocked) (Figure 2M). In contrast, *Zfp423* deletion alone robustly increased uncoupled respiration (oligomycin resistant), including UCP1-dependent uncoupling, independent of the presence of T3 (Figure 2N). In *Zfp423*-ablated adipocytes stimulated with NE for 24 h prior to measurement, uncoupled respiration was enhanced by T3, indicating that T3 was required for the full thermogenic response to adrenergic activation (Figure 2N). Notably, maximal capacity (FCCP induced) was also increased in *Zfp423*-ablated adipocytes, which was dependent on T3 in the absence of NE stimulation (Figure 2O). Altogether, these data recapitulate the importance of intact TH signaling for activation of UCP1-dependent thermogenesis in beige adipocytes of *Zfp423iAKO* mice, leading to increased energy expenditure and a stabilization of body temperature at lower ambient temperatures.

Signal transduction downstream of β AR activation in beige adipocytes depends on thyroid hormones

To get further insights how adrenergic signaling in iWAT of *Zfp423iAKO* mice is coupled to TH signaling, we administered NE (1 μ g per g body weight) to fully stimulate adaptive thermogenesis (Figure 3A). Consistent with the established role of THs in thermogenesis, NE treatment induced a significantly greater increase in oxygen consumption in euthyroid mice compared to hypothyroid mice (Figures 3B and 3C). In accordance with our prior observation, basal oxygen consumption prior to NE injection was increased in euthyroid *Zfp423iAKO* mice compared to euthyroid controls. However, NE-stimulated oxygen consumption was comparable in both groups (Figures 3B and 3C). This may be due to full activation of BAT thermogenesis overriding the thermogenic activity of iWAT, as acute NE treatment increased BAT and body temperature in euthyroid mice (Figures 3D and 3E). Notably, maximal response to NE occurred approximately 10 min earlier in *Zfp423iAKO* than in control mice regardless of TH status, indicating an increased adrenergic sensitivity (Figure 3F). To examine potential receptor effects, *Adrb1* and *Adrb3* mRNA expression was measured in iWAT, gWAT, and BAT of all experimental groups at all temperatures (Figures 3G and S3A–S3C). Only *Adrb1* levels in the iWAT depot were increased in both euthyroid and hypothyroid *Zfp423iAKO* mice, possibly explaining the increased sensitivity (Figure 3G). However, *Zfp423*-ablated primary adipocytes isolated from iWAT showed increased expression of both *Adrb1* and *Adrb3* (Figure S3D). Furthermore, the β 3AR-specific activator CL-316243 induced uncoupled respiration in these cells at levels comparable to those induced by NE (Figure S3E). The finding

that β AR expression in the iWAT of *Zfp423iAKO* mice was regulated independent of TH, whereas uncoupled respiration and energy expenditure depended on TH, indicates impaired signal transduction downstream of β AR in the absence of TH (Figure 3H). Accordingly, cAMP levels and phosphorylation of hormone-sensitive lipase (HSL) were increased in iWAT of euthyroid but not hypothyroid *Zfp423iAKO* mice compared to controls at 18°C (Figures 3I and 3J). We further examined this at the cellular level by measuring uncoupled respiration in response to either NE-mediated β AR activation or forskolin-mediated adenylyl cyclase activation (Figures 3H and 3K). In the presence of T3, *Zfp423*-ablated adipocytes displayed a significantly higher uncoupling response to both NE and forskolin (FSK) compared to control adipocytes. This effect was completely absent under T3 deficient conditions, even when cAMP production was stimulated by FSK (Figure 3L). This indicates that NE-stimulated uncoupling may be impaired by increased cAMP turnover under T3-deficient conditions.²³ This is supported by the observation that preincubation with the nonspecific phosphodiesterase inhibitor IBMX significantly increased the OCR of *Zfp423*-ablated adipocytes, leading to higher basal respiration in both T3-treated and T3-deficient *Zfp423*-ablated adipocytes (Figures 3M and 3N). Taken together, our data indicate that beige adipocytes formed in response to *Zfp423* deletion display increased adrenergic sensitivity, possibly due to β AR upregulation. However, the thermogenic response to adrenergic activation is critically dependent on THs, which influence the signal transduction downstream of β AR.

Thyroid hormone-dependent iWAT browning and increased energy expenditure are mediated by TR β signaling

Next, we aimed to examine the underlying pathways that ultimately link TH signaling to thermogenic activation of beige adipose tissue. Since UCP1 expression in iWAT is dependent on TR β ,¹² and targeted activation of TR β leads to WAT browning in parallel with increases in energy expenditure and body temperature,¹³ we questioned whether TR β activation is sufficient to activate beige thermogenesis in *Zfp423iAKO* mice. To this end, we treated hypothyroid *Zfp423iAKO* and hypothyroid control mice with two different doses of the TR β -specific agonist GC-1: a lower dose that has been described as equimolar to the T3 dose needed to normalize plasma and tissue TH levels in hypothyroid mice^{24,25} (1.8 ng/g/day, 10 days; Figure 4A) and a higher (supraphysiological) dose that has been used by Lin et al.¹³ (300 ng/g/day, 14 days; Figure 4F). TR β activation was confirmed by hepatic mRNA expression of the T3-responsive gene *Dio1*, which was significantly increased in GC-1-treated mice compared to saline-treated mice (Figures S4A and S4D). The lower dose of GC-1 enhanced the increase in UCP1 expression in iWAT of *Zfp423iAKO* mice, whereas *Zfp423* mRNA and UCP1 levels in control mice remained unaffected (Figures 4B–4E and S4B). Notably, the higher dose of GC-1 reduced *Zfp423* expression in iWAT and gWAT of control mice compared to saline-treated controls (Figures 4F and 4G). In iWAT, this was accompanied by a significant increase in UCP1 protein, which was even more pronounced in *Zfp423iAKO* mice (Figures 4H–4J and S4E). In gWAT, neither

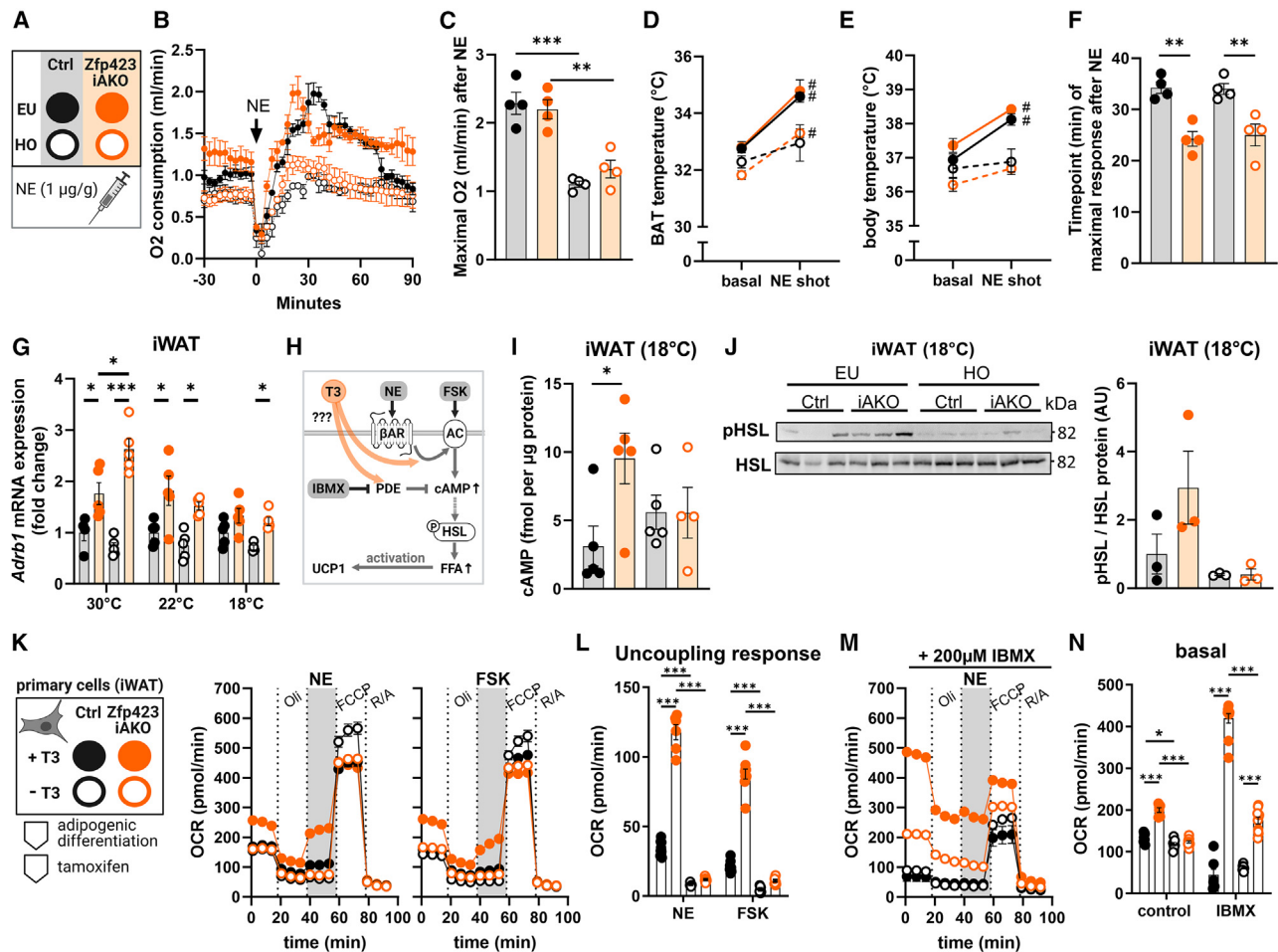


Figure 3. Signal transduction downstream of β AR activation in beige adipocytes depends on thyroid hormones

(A) Female Zfp423iAKO mice and floxed littermate controls (Ctrl) were rendered euthyroid (EU) and hypothyroid (HO) and treated with tamoxifen as described in Figure 1A. At the end of treatment, norepinephrine (NE; 1 μ g/g, subcutaneously) was acutely injected.

(B) Oxygen consumption progress from 30 min before to 90 min after NE injection. $n = 4$.

(C) Maximal value of oxygen consumption measured after NE injection. $n = 4$.

(D and E) (D) Temperature of BAT calculated from infrared thermography and (E) body temperature measured before and after NE injection. $n = 5$. The # symbol denotes significance between basal and NE conditions (Sidak multiple-comparisons test).

(F) Time after NE injection when maximal oxygen consumption was reached. $n = 4$.

(G) *Adrb1* mRNA expression in iWAT of mice at different housing temperatures, represented as fold change to the Ctrl/EU group. $n = 4-5$.

(H) Schematic view of the β -adrenergic signaling cascade and potential points for T3 to intervene.

(I) cAMP levels in iWAT of mice held at 18°C. $n = 4-5$.

(J) Western blot of pHSL and HSL protein expression in iWAT of mice held at 18°C. Signal ratio was calculated and represented as fold change to the Ctrl/EU group. $n = 3$.

(K) Stromal vascular cells isolated from iWAT of Zfp423iAKO and control mice were differentiated in TH-depleted medium with or without 10 nM T3. Zfp423 deletion was induced by treatment with 1 μ M tamoxifen for 48 h. After 48 h of washout, OCR was measured after stimulation with 2 μ M Oli, 2.5 μ M FCCP (CAS: 370-86-5), 5 μ M NE or forskolin (FSK), and 0.5 μ M R/A. Three mice per genotype (Ctrl/Zfp423iAKO) were pooled and measured in technical replicates. $n = 8-12$.

(L) Uncoupling response calculated as (maximal OCR after NE/FSK) - (minimal OCR after Oli).

(M) OCR progress after pre-incubation with 200 μ M 3-Isobutyl-1-methylxanthin (IBMX) for 45 min

(N) Basal respiration calculated as (basal OCR) - (minimal OCR after R/A).

Data are presented as mean \pm SEM. Two-way ANOVA with Tukey post hoc test for multiple comparisons. * $p < 0.05$, ** $p < 0.01$, *** $p < 0.001$. See also Figure S3.

dose of GC-1 significantly altered UCP1 protein levels in control or Zfp423iAKO mice (Figures 4D and 4I). Importantly, TR β activation with the lower dose of GC-1 was sufficient to increase energy expenditure in hypothyroid Zfp423iAKO mice ($p = 0.020$) but not in hypothyroid controls ($p = 0.899$) at room tem-

perature (Figures 4K and S4C; Table S3). While body temperature and BAT temperature remained unchanged, tail temperature was increased in GC-1-treated Zfp423iAKO mice compared to GC-1-treated controls (Figures 4L and 4M). This suggests that Zfp423iAKO mice increase heat dissipation

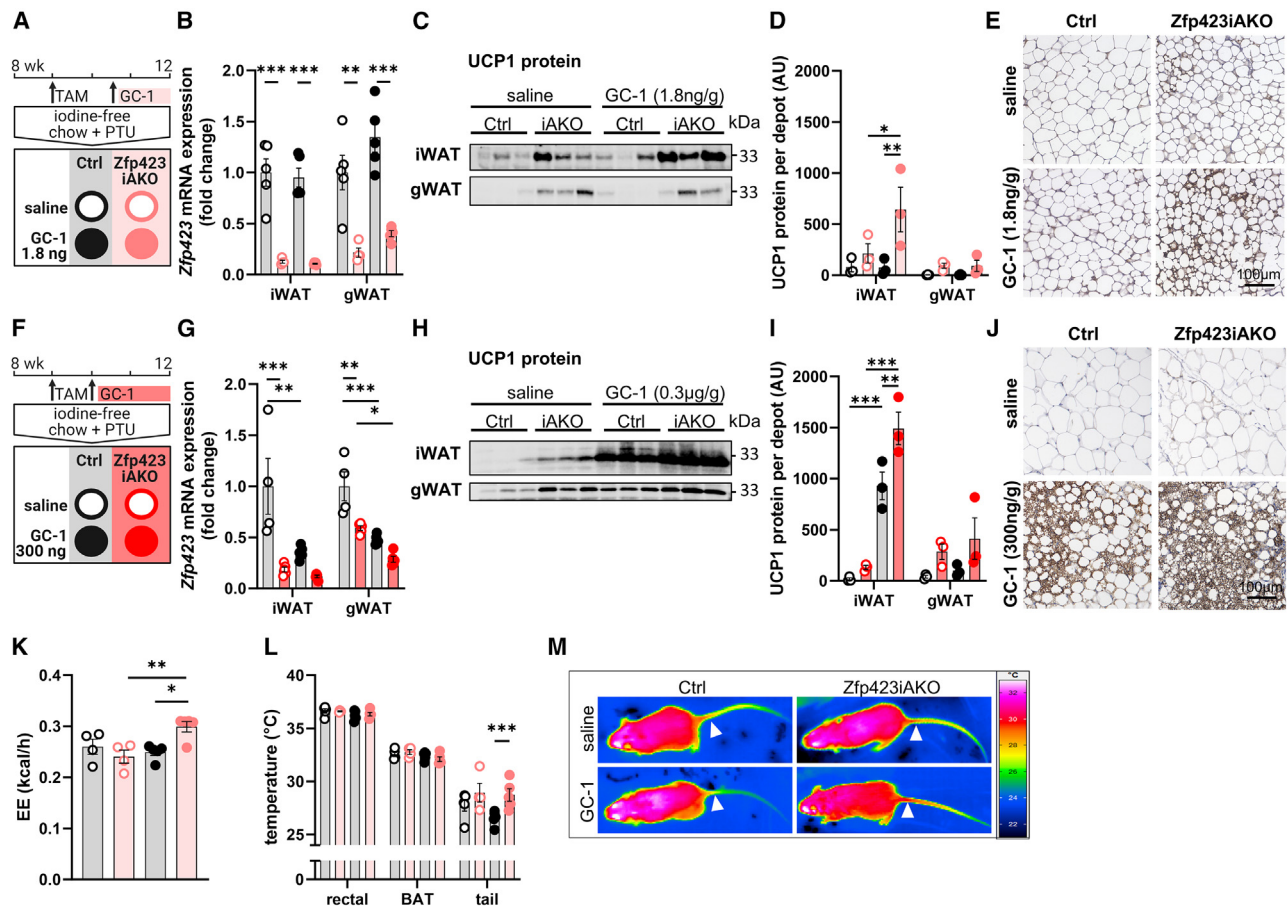


Figure 4. Thyroid hormone-dependent iWAT browning and increased energy expenditure are mediated by TR β signaling
 (A and F) Female Zfp423iAKO mice and floxed littermate controls (Ctrl) were rendered hypothyroid by feeding a iodine-free chow diet complemented with 0.15% PTU for 4 weeks and were treated with tamoxifen as described in Figure 1A. During the last days of treatment, mice were injected with saline control or GC-1 at a lower dose (A; 1.8 ng/g, i.p., 10 days) or higher dose (F; 300 ng/g, i.p., 14 days).
 (B and G) Zfp423 mRNA expression in iWAT and gWAT after treatment with a (B) low or (G) high dose of GC-1, represented as fold change to the Ctrl/saline group. $n = 4-5$.
 (C and H) Western blot of UCP1 protein expression in iWAT and gWAT after treatment with a (C) low or (H) high dose of GC-1. $n = 3$. Signal intensity was normalized to total protein (Figures S4B and S4E).
 (D and I) Total UCP1 protein amount per adipose tissue depot after treatment with a (D) low or (I) high dose of GC-1. $n = 3$.
 (E and J) Immunohistochemical staining of UCP1 in iWAT sections after treatment with a (E) low dose of GC-1 (representative images, $n = 3$) or (J) high dose of GC-1 (representative images, $n = 4$).
 (K) Mean energy expenditure after treatment with a low dose of GC-1. $n = 4$. See Figure S4C and Table S3 for statistical analysis.
 (L and M) Rectal body temperature, BAT temperature, and tail temperature measured 0.5 cm from the tail base of mice treated with a low dose of GC-1. Values were calculated from infrared thermography as depicted in representative images in (M). $n = 4-5$.
 Data are presented as mean \pm SEM. Two-way ANOVA with Tukey post hoc test for multiple comparisons. * $p < 0.05$, ** $p < 0.01$, *** $p < 0.001$. See also Figure S4 and Table S3.

through tail vasodilation in response to excess heat generated by iWAT thermogenesis following TR β activation. Collectively, these data demonstrate that TR β signaling mediates the UCP1-dependent thermogenic activity of beige adipocytes within the iWAT depot of Zfp423iAKO mice.

Thyroid hormone signaling is coupled to ZFP423-regulated pathways to control thermogenic programs of beige adipocytes

ZFP423 exerts its anti-thermogenic effect by impairing EBF2-regulated transcriptional activities.^{16,17} We were interested

whether TR β signaling interplays with this pathway in controlling iWAT thermogenesis. To this end, we analyzed a recently described enhancer -5.8 kb upstream of the *Ucp1* gene, which is synergistically activated by EBF2 and PPAR γ coactivator 1 α (PGC1 α).²⁶ Binding motif analysis revealed two putative binding motifs for TR β within this enhancer. Using luciferase reporter gene assays, we first confirmed the transcriptional activation by EBF2 and PGC1 α (Figure 5A). Co-transfection with ZFP423 suppressed this activation, consistent with its inhibitory effect on EBF2 (Figure 5A). To elucidate the role of TH signaling, TR β and TR α were co-expressed, and cells were maintained under

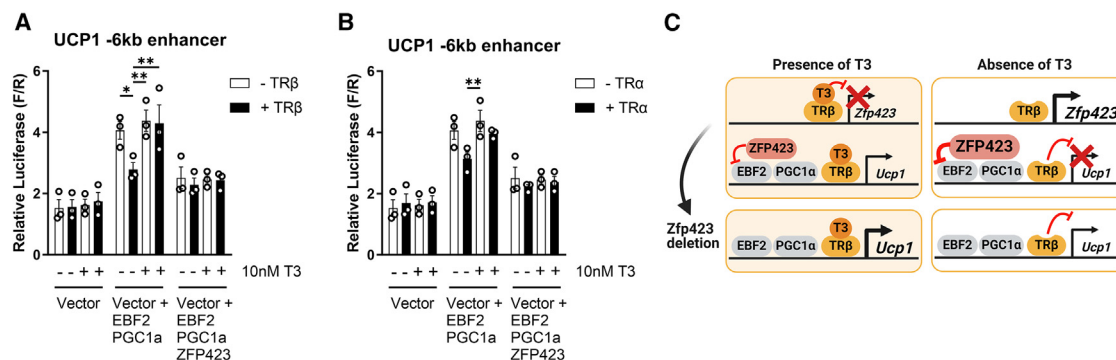


Figure 5. Thyroid hormone signaling is coupled to ZFP423-regulated pathways to control thermogenic programs of beige adipocytes

(A and B) Firefly luciferase activity normalized to *Renilla* luciferase activity in 3T3-L1 cells transfected with the pGL4.23_Ucp1 -6kb enhancer plasmid and expression plasmids of EBF2, PGC1 α , ZFP423, and (A) TR β or (B) TR α as indicated. Cells were held under TH-depleted conditions supplemented with or without 10 nM. $n = 3$ biological replicates and 2 technical replicates. Data are presented as mean \pm SEM. Two-way ANOVA with Tukey post hoc test for multiple comparisons. * $p < 0.05$, ** $p < 0.01$, *** $p < 0.001$.

(C) Proposed model for the coupling of TH signaling and Zfp423 signaling pathways in the thermogenic control of beige adipocytes.

See also Figure S4.

TH-depleted conditions supplemented with solvent or 10 nM T3. The functionality of this system was confirmed by a p(DR4)2 control reporter (Figure S4F). Notably, the unliganded TR β inhibited the EBF2/PGC1 α activation to a similar extent as ZFP423, which was reversed by stimulation with T3 (Figure 5A). This effect was less pronounced with cotransfection of TR α (Figure 5B). Collectively, these data provide functional evidence that T3 binding to TRs is necessary for the EBF2-mediated transcriptional activation of the *Ucp1* gene. Combining these data with the *in vivo* data, we propose a model for the thermogenic control of beige adipocytes that couples TH signaling and ZFP423 signaling pathways (Figure 5C). TH-induced TR β activation transcriptionally regulates the amount of ZFP423 available to inhibit the activity of EBF2. EBF2 synergizes with PGC1 α to activate thermogenic gene expression, which is suppressed by the unliganded TR β in the absence of T3. Therefore, both the inactivation of ZFP423 and the presence of T3 are required to fully stimulate the thermogenic gene program.

Expression of *THRs*, *ZNF423*, and *UCP1* are associated in human adipose tissue

To elucidate whether ZNF423 (the human ortholog of ZFP423) and TR signaling interact to influence human adipose tissue plasticity, we analyzed abdominal subcutaneous adipose tissue (SAT) and omental visceral adipose tissue (VAT) samples from the Leipzig Obesity Biobank (LOBB). *ZNF423* mRNA levels were significantly higher in VAT of obese patients compared to paired SAT (Figure 6A). Due to the lack of intracellular T3 levels, it is not known whether TRs in the human samples are liganded. However, as we observed an increased *Thra/Thrb* mRNA expression in iWAT and gWAT of hypothyroid controls compared to euthyroid controls, we assume an inverse correlation between TR expression and ligand availability (Figure 6B). *ZNF423* expression correlated positively with *THRA* and *THRB* levels (Figures 6C and 6D). Based on the assumption of mostly unliganded TRs, these data suggest that *ZNF423* expression in human adipose tissue may be negatively regulated by THs, similar

to our previous observation in mice.¹⁴ Furthermore, expression of the thermogenic genes *UCP1* and *PRDM16* correlated negatively with *ZNF423*, *THRA*, and *THRB* (Figure 6E). Mediation analysis further suggests that the negative association of *THRA* and *THRB* with *UCP1* expression was partially mediated by *ZNF423* (Table 1). In conclusion, the LOBB dataset gives initial evidence that the interplay between ZNF423 and TH signaling could be of relevance in human adipose depots. Future studies are warranted to validate this hypothesis and to investigate the potential of a TR-based targeted approach to control systemic energy metabolism in humans.

DISCUSSION

The broad effects of THs on basal metabolism and adaptive thermogenesis make them ideal integrators for different metabolic signals. However, the study of TH-driven thermoregulatory circuits is challenging, since THs regulate thermogenesis through peripheral and central pathways in a complex interplay with the sympathetic nervous system. Studies of hyperthyroid humans and mice have shown that increased energy expenditure in systemic hyperthyroidism can be mainly attributed to T3-induced heat production in skeletal muscle but not in adipose tissue.^{12,27–29} Nevertheless, the targeted activation of TH signaling by glucagon-mediated T3 delivery to adipocytes³⁰ and TR β agonist treatment¹³ increased whole-body energy expenditure due to induction of adaptive thermogenesis in white adipose depots. Based on these studies, we aimed to investigate the molecular mechanism by which TH signaling drives adaptive thermogenesis in beige adipocytes.

Our recent finding that THs directly regulate *Zfp423* expression through TR isoform-specific signaling in distinct adipose depots¹⁴ adds a new perspective to the involvement of THs in beige adipose tissue development and activation. Downregulation of the anti-thermogenic transcription factor ZFP423 is a central node in the cold-induced recruitment of beige adipocytes.¹⁶ Mechanistically, ZFP423 binds to EBF2 and recruits a

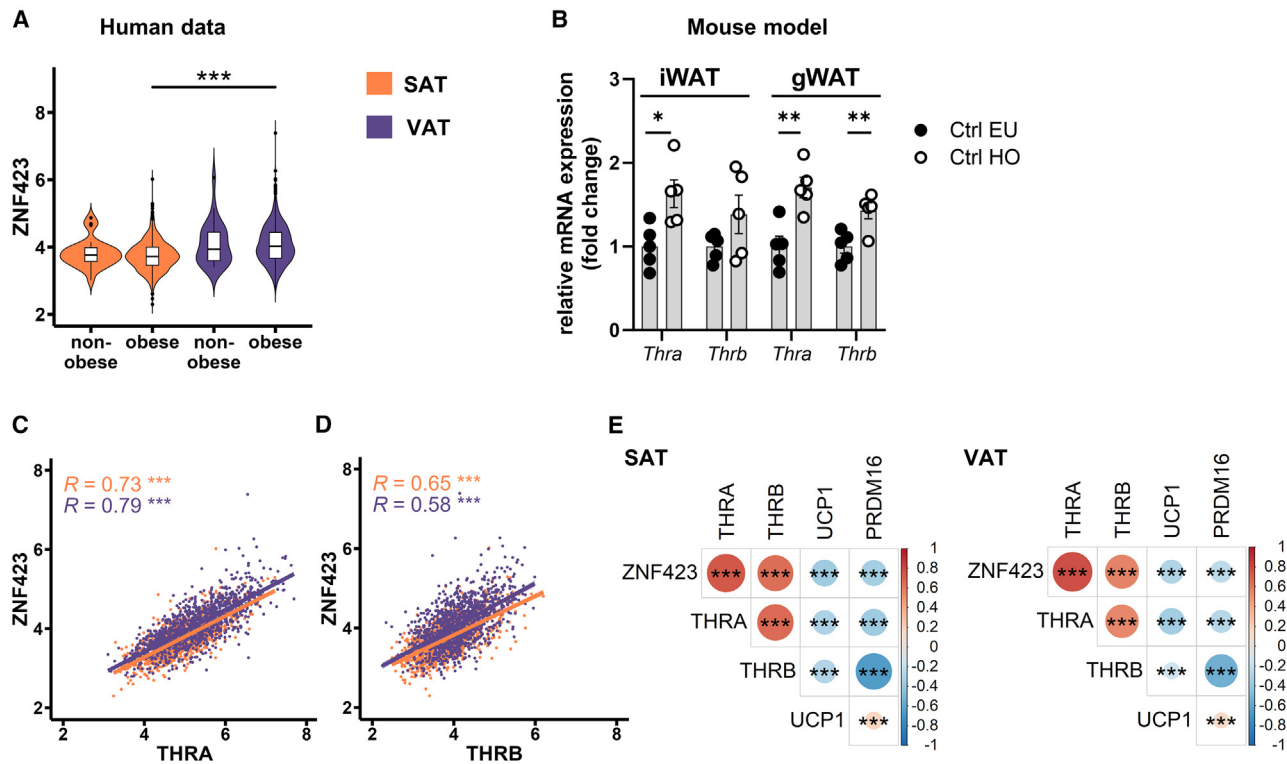


Figure 6. Expression levels of THRs, ZNF423, and UCP1 are associated in human adipose tissue

(A) Expression level of *ZNF423* in paired subcutaneous adipose tissue (SAT) and visceral adipose tissue (VAT) samples of 1,176 obese and 26 non-obese individuals of the LOBB. Shown is a violin plot with a boxplot depicting minima, first quartile, median, third quartile, and maxima. Median \pm SD: 3.77 ± 0.425 (SAT non-obese), 3.72 ± 0.433 (SAT obese), 3.94 ± 0.625 (VAT non-obese), 4.02 ± 0.562 (VAT obese). Dunn's test for non-parametric pairwise multiple comparison with Holm *p* value adjustment.

(B) *Thra* and *Thrb* mRNA expression in iWAT and gWAT of eu- and hypothyroid control mice, represented as fold change to the Ctrl/EU group. *n* = 5. Data are represented as mean \pm SEM. Student's *t* test.

(C and D) Spearman correlation between *ZNF423* and (C) *THRA* or (D) *THRB* in human SAT and VAT samples with a confidence interval of 0.95.

(E) Gene correlation matrix of *ZNF423*, *THRA*, *THRB*, *UCP1* and *PRDM16* in human SAT and VAT. The calculation was based on Spearman correlation coefficient and a confidence interval of 0.95.

p* < 0.05, *p* < 0.01, ****p* < 0.001.

co-repressor complex to EBF2-bound thermogenic gene enhancers. Upon the loss of ZFP423, the repressor is exchanged for a transcriptional activator, leading to the induction of the thermogenic gene program.¹⁷ Here, we postulate that THs act on this system via TR β as a central switch by two different mechanisms. (1) TR β activation represses *Zfp423* transcription, thereby reducing the amount of ZFP423 available to disrupt the EBF2 co-activator complex. (2) TR β binds to a TH-responsive element within -5.8 kb of the *Ucp1* enhancer,²⁶ thereby facilitating EBF2/PGC1 α -mediated transcription upon T3 binding. The functional relationship was confirmed by luciferase reporter gene assays. Notably, this approach cannot completely exclude the potential involvement of TR α . A recent chromatin immunoprecipitation/RNA sequencing (RNA-seq) meta-analysis furthermore substantiated the binding of TRs to the -5.8 kb region upstream of the *Ucp1* gene in adipose tissue in both the absence and presence of systemic THs.³¹ It is therefore likely that this enhancer is physiologically relevant for TH action on the *Ucp1* gene in addition to the well-known T3- and cAMP-responsive enhancer -2.4 kb upstream.³² It remains open how

the unliganded TR β represses EBF2/PGC1 α -mediated transcription. Possibly, it impairs the recruitment of PGC1 α to the activator complex since PGC1 α interacts with TR β only in the presence of T3.³³ In addition, unliganded TRs induce histone deacetylation through binding of corepressors and histone deacetylase 3, which might impede the EBF2-mediated gene activation.³⁴ With regard to our *in vivo* data, the interplay of ZFP423 and TH-mediated signaling provides a functional framework for TR β -induced WAT browning. Thus, treatment of hypothyroid control mice with a supraphysiological dose of GC-1, which has been shown by Lin et al.¹³ to increase energy expenditure dependent on increased UCP1 expression in iWAT, was paralleled by significantly suppressed *Zfp423* mRNA levels. Contrarily, a low dose of GC-1 did not alter *Zfp423* expression, and both UCP1 levels and energy expenditure remained unaffected. Upon *Zfp423* inactivation, however, the low dose of GC-1 sufficed to increase UCP1 protein expression in iWAT. The concomitant increase in energy expenditure confirms that beige adipocytes in *Zfp423iAKO* mice were thermogenically active and produced even more heat than required to meet the

Table 1. Mediation analysis of gene expression in SAT and VAT samples of the LOBB

Tissue	IV	DV	Med	Effect			Stage	
				Total	Direct	Indirect	IV > Med	Med > Dep
SAT	THRA	UCP1	ZNF423	−0.18 ***	−0.04.	−0.14 ***	0.54 ***	−0.26 ***
SAT	THRB	UCP1	ZNF423	−0.20 ***	−0.09 ***	−0.11 ***	0.49 ***	−0.23 ***
VAT	THRA	UCP1	ZNF423	−0.19 ***	−0.17 ***	−0.02	0.54 ***	−0.03
VAT	THRB	UCP1	ZNF423	−0.08 ***	0.07 *	−0.14 ***	0.55 ***	−0.26 ***

Linear mixed regression between independent variable (IV), dependent variable (DV), and mediator (Med). Nonparametric bootstrap confidence intervals were constructed using the percentile method and 1,000 resamples. .<0.1; * $p < 0.05$; ** $p < 0.01$; *** $p < 0.001$. See also Figure 6.

body temperature set point, as indicated by enhanced heat loss over the tail surface. Thus, we provide a proof of principle showing that THs regulate both UCP1 expression and thermogenic activation of beige adipocytes through the TR β isoform. This is in contrast to brown adipocytes of hypothyroid mice, where TR β activation restored UCP1 levels but failed to normalize the thermogenic response to NE.³⁵ Studies with TR β KO mice further showed that TR β is indispensable for T3-mediated UCP1 expression in iWAT but not in BAT.¹² Notably, we observed this central role of TR β only in *Zfp423*-ablated beige adipocytes of the inguinal depot, whereas UCP1 expression in the gonadal depot appeared to be virtually unaffected by targeted TR β agonism as well as systemic TH status. This is reminiscent of our previous study showing that TR β is required for downregulation of *Zfp423* expression only in iWAT but not in gWAT or BAT.¹⁴

Adrenergic activation through cold exposure or β AR agonist treatment is the key driver of beige adipocyte recruitment.³⁶ However, a recent study by Guilherme et al.³⁷ demonstrated that adrenergic activation alone is not sufficient to induce UCP1 expression in iWAT of hypothyroid mice, a scenario also reflected by our data in control mice. Contrarily, TR β agonist treatment increased iWAT browning and energy expenditure even in the virtual absence of sympathetic signaling at 30°C.¹³ *Zfp423*iAKO mice represent an optimal model to study the distinct effects of TH and NE signaling in beige adipocytes on both thermogenic capacity and thermogenic activation, as they express detectable UCP1 protein levels in iWAT at 30°C and in the hypothyroid status. Here, we show that THs are mandatory to fully activate UCP1 expression as well as UCP1-dependent thermogenic activity in beige adipocytes. Notably, UCP1 protein expression in iWAT of euthyroid *Zfp423*iAKO mice was increased to levels comparable to BAT, reflecting the extraordinarily high thermogenic capacity of beige adipocytes in these mice. Energy expenditure was exclusively increased in euthyroid but not in hypothyroid *Zfp423*iAKO mice irrespective of ambient temperature. The effect was entirely driven by WAT thermogenesis, since UCP1-dependent thermogenesis in BAT was not altered in *Zfp423*iAKO mice, and BAT-targeted *Zfp423* deletion did not affect energy expenditure. Sympathetic stimulation, however, failed to increase energy expenditure in hypothyroid *Zfp423*iAKO mice despite the presence of UCP1 protein. Consistently, the NE-stimulated increase in uncoupled mitochondrial respiration of *Zfp423*-ablated adipocytes was completely blocked in the absence of T3. Our observations

share features with earlier landmark experiments in BAT, demonstrating that UCP1 response to adrenergic activation is blunted in hypothyroid rats and restored following T4 treatment.⁷ The molecular causes are not yet fully understood and range from abnormalities at the receptor and adenylate cyclase level to changes in phosphodiesterase activity.^{4,5,23,38} Data from our *Zfp423*iAKO model suggest that the impaired thermogenic activity under TH deficiency is likely caused by increased cAMP turnover. This is evidenced by *Adrb1* upregulation in iWAT of *Zfp423*iAKO mice regardless of TH status, possibly leading to increased adrenergic sensitivity but activation of downstream signaling only in euthyroid *Zfp423*iAKO mice. In addition, oxygen consumption in T3-deficient *Zfp423*-ablated adipocytes was partially restored by inhibition of phosphodiesterase (cAMP degradation) but not by activation of adenylate cyclase (cAMP production). In summary, our analyses uncovered that THs are critical for full UCP1-dependent thermogenic response to adrenergic activation in beige adipocytes.

Altogether, our work establishes ZFP423 as a TH-driven relay that couples changes in adipocyte phenotype to changes in adaptive thermogenesis as a mechanism of adaptation to physiological demands. THs modulate the ZFP423-EBF2-UCP1 axis through multiple transcriptional pathways, with TR β playing a central role, particularly in the inguinal depot. Moreover, THs were found to be essential for UCP1-dependent thermogenic activation of beige adipocytes.

In humans, hypothyroidism is associated with hepatic steatosis, weight gain, and increased risk of cardiovascular diseases, reflecting the physiological relevance of THs for multiple metabolic pathways.^{39–41} In the human LOBB cohort, *ZNF423* levels were higher in the visceral depot compared to the subcutaneous depot. In congruence with our previous data in mice,¹⁴ we found first evidence that *ZNF423* expression in human adipose tissue may be regulated by THs. Correlation analyses indicated a potential interaction between *ZNF423* and TRs in the transcriptional control of thermogenic genes such as *UCP1*, though further functional evidence is clearly needed. However, these findings open up therapeutic perspectives for combating obesity and metabolic disorders by modulating the thermogenic properties in human adipose tissue via TR-targeted approaches. Recently, a phase 3 report demonstrated beneficial effects of the oral TR β -agonist resmetirom on liver fibrosis.⁴² Additional research on the mechanisms underlying inter-organ actions of THs with effects on lipid metabolism and thermogenesis will be of great interest to the field.

Limitations of the study

In order to examine the role of TH and NE signaling for the regulation of beige adipocytes, we utilized the *Zfp423iAKO* mouse as a potent model of WAT browning. Thus, our experimental setup is limited to beige adipocytes that were converted from adiponectin-expressing mature adipocytes in response to *Zfp423* inactivation. Our attempt to focus on these cells arose from earlier observations showing that *Zfp423* is targeted and regulated by TH. However, the current state of research emphasizes the existence of a variety of cold-responsive cell types that drive thermogenesis in WAT. Furthermore, this work focused on UCP1-dependent thermogenesis in beige adipocytes. Further research on the involvement of TH in UCP1-independent thermogenic processes, such as ATP-consuming futile creatine cycles and others,^{43,44} will be of great interest to the field. In the human LOBB cohort, the majority of paired tissue samples were derived from obese individuals. Due to a lack of data on intracellular T3 levels, we estimated the activation status of TRs based on the expression of T3-sensitive marker genes (data not shown), which was supported by data from human primary cells (data not shown) and a separate mouse model of TH deficiency. All assumptions regarding regulatory mechanisms were based on gene correlation analysis and need further functional validation.

RESOURCE AVAILABILITY

Lead contact

Requests for further information, resources, and reagents should be directed to and will be fulfilled by the lead contact, Kerstin Krause (kerstin.krause@medizin.uni-leipzig.de).

Materials availability

This study did not generate new unique reagents.

Data and code availability

The human RNA-seq data reported in this study were generated from samples of the LOBB and cannot be deposited in a public repository because of patient consent restrictions. These restrictions are due to local data protection regulation in the written informed consent form tissue donors signed before taking part in the study. Access to human adipose tissue bank data is regulated by the LOBB steering committee. Use of data is strictly limited to research purposes and not intended for commercialization. To request access, contact Matthias Blüher (bluma@medizin.uni-leipzig.de) or Anne Hoffmann (anne.hoffmann@helmholtz-munich.de). Summary statistics describing the dataset used in this study can be found in the [STAR Methods](#). All other data reported in this paper will be shared by the [lead contact](#) upon request. All software and packages applied are publicly available and listed in the [key resources table](#). This paper does not report original code. Any additional information required to reanalyze the data reported in this paper is available from the [lead contact](#) upon request.

ACKNOWLEDGMENTS

This work was funded by the German Research Foundation (DFG; KR 4258/3-1 to K. Krause) and through SFB1052, project number 209933838, subprojects B1, B12, C6, and C7. The work was also funded by the Free State of Saxony and Helmholtz Munich (to M.B.). The German Diabetes Center is funded by the German Federal Ministry of Health (Berlin, Germany) and the Ministry of Culture and Science of the state of North Rhine-Westphalia (Düsseldorf, Germany) and receives additional funding from the German Federal Ministry of Education and Research (BMBF) through the German Center for Diabetes Research (DZD e.V.). We thank Wenfei Sun and Hua Dong for supporting human adipose

tissue RNA-seq. We further thank all patients and their families for participating in the Leipzig Obesity BioBank (LOBB). Schematic figures were created with [BioRender](#) (agreements TP278UA24T, AI278UA29L, AQ278UA2BP, TP278UA2EI, XX278UA2GR, UB278UA2JR, GI278UA2M9, NC278UA2OS, and SZ278UA2QS).

AUTHOR CONTRIBUTIONS

L.R. performed conceptualization, experimental work, data analysis and interpretation, visualization, and writing and editing of the manuscript. M.B. and C.W. contributed human data. A.G. and F.N. performed RNA-seq of samples from the Leipzig Obesity Biobank. A.H. and T.H. performed bioinformatics. L.W., C.S., B.S., L.D., K. Krohn, J.W., J.T.H., and N.K. contributed to experimental work and provided materials. A.T. and M.S. reviewed and edited the manuscript. J.M. contributed to data interpretation and edited the manuscript. K. Krause was responsible for conceptualization, supervision, validation, data analysis and interpretation, and writing and editing of manuscript. All authors commented on the manuscript.

DECLARATION OF INTERESTS

M.B. received honoraria as a consultant and speaker from Amgen, AstraZeneca, Bayer, Boehringer-Ingelheim, Lilly, Novo Nordisk, Novartis, and Sanofi, which had no role in the conducting of this study.

STAR★METHODS

Detailed methods are provided in the online version of this paper and include the following:

- [KEY RESOURCES TABLE](#)
- [EXPERIMENTAL MODEL AND STUDY PARTICIPANT DETAILS](#)
 - Human cohort
 - Animals
 - Primary cell culture
 - Cell lines
- [METHOD DETAILS](#)
 - Bulk RNA sequencing and analysis of human data
 - Metabolic phenotyping of mice
 - Infrared thermography
 - ELISA
 - Western Blot analysis
 - Immunohistochemistry
 - Oxygen consumption assay in primary adipocytes
 - Gene expression analysis
 - Luciferase gene reporter assay
- [QUANTIFICATION AND STATISTICAL ANALYSIS](#)

SUPPLEMENTAL INFORMATION

Supplemental information can be found online at <https://doi.org/10.1016/j.celrep.2024.114987>.

Received: March 20, 2024

Revised: August 30, 2024

Accepted: October 31, 2024

REFERENCES

1. Mullur, R., Liu, Y.-Y., and Brent, G.A. (2014). Thyroid hormone regulation of metabolism. *Physiol. Rev.* *94*, 355–382. <https://doi.org/10.1152/physrev.00030.2013>.
2. Silva, J.E. (2011). Physiological importance and control of non-shivering facultative thermogenesis. *Front. Biosci.* *3*, 352–371. <https://doi.org/10.2741/s156>.

3. Silva, J.E., and Larsen, P.R. (1983). Adrenergic activation of triiodothyronine production in brown adipose tissue. *Nature* 305, 712–713. <https://doi.org/10.1038/305712a0>.
4. Rubio, A., Raasmaja, A., Maia, A.L., Kim, K.R., and Silva, J.E. (1995). Effects of thyroid hormone on norepinephrine signaling in brown adipose tissue. I. Beta 1- and beta 2-adrenergic receptors and cyclic adenosine 3',5'-monophosphate generation. *Endocrinology* 136, 3267–3276. <https://doi.org/10.1210/endo.136.8.7628360>.
5. Carvalho, S.D., Bianco, A.C., and Silva, J.E. (1996). Effects of hypothyroidism on brown adipose tissue adenylyl cyclase activity. *Endocrinology* 137, 5519–5529. <https://doi.org/10.1210/endo.137.12.8940379>.
6. Cannon, B., and Nedergaard, J. (2004). Brown adipose tissue: function and physiological significance. *Physiol. Rev.* 84, 277–359. <https://doi.org/10.1152/physrev.00015.2003>.
7. Bianco, A.C., and Silva, J.E. (1987). Intracellular conversion of thyroxine to triiodothyronine is required for the optimal thermogenic function of brown adipose tissue. *J. Clin. Invest.* 79, 295–300. <https://doi.org/10.1172/JCI112798>.
8. Shapira, S.N., and Seale, P. (2019). Transcriptional Control of Brown and Beige Fat Development and Function. *Obesity* 27, 13–21. <https://doi.org/10.1002/oby.22334>.
9. Shao, M., Wang, Q.A., Song, A., Vishvanath, L., Busbuso, N.C., Scherer, P.E., and Gupta, R.K. (2019). Cellular Origins of Beige Fat Cells Revisited. *Diabetes* 68, 1874–1885. <https://doi.org/10.2337/db19-0308>.
10. Weiner, J., Kranz, M., Klötting, N., Kunath, A., Steinhoff, K., Rijntjes, E., Köhrle, J., Zeisig, V., Hankir, M., Gebhardt, C., et al. (2016). Thyroid hormone status defines brown adipose tissue activity and browning of white adipose tissues in mice. *Sci. Rep.* 6, 38124. <https://doi.org/10.1038/srep38124>.
11. Martínez-Sánchez, N., Moreno-Navarrete, J.M., Contreras, C., Rial-Pensado, E., Fernø, J., Nogueiras, R., Diéguez, C., Fernández-Real, J.-M., and López, M. (2017). Thyroid hormones induce browning of white fat. *J. Endocrinol.* 232, 351–362. <https://doi.org/10.1530/JOE-16-0425>.
12. Johann, K., Cremer, A.L., Fischer, A.W., Heine, M., Pensado, E.R., Resch, J., Nock, S., Virtue, S., Harder, L., Oelkrug, R., et al. (2019). Thyroid-Hormone-Induced Browning of White Adipose Tissue Does Not Contribute to Thermogenesis and Glucose Consumption. *Cell Rep.* 27, 3385–3400.e3. <https://doi.org/10.1016/j.celrep.2019.05.054>.
13. Lin, J.Z., Martagón, A.J., Cimini, S.L., Gonzalez, D.D., Tinkey, D.W., Biter, A., Baxter, J.D., Webb, P., Gustafsson, J.Å., Hartig, S.M., and Phillips, K.J. (2015). Pharmacological Activation of Thyroid Hormone Receptors Elicits a Functional Conversion of White to Brown Fat. *Cell Rep.* 13, 1528–1537. <https://doi.org/10.1016/j.celrep.2015.10.022>.
14. Roth, L., Johann, K., Hönes, G.S., Oelkrug, R., Wagner, L., Hoffmann, A., Krohn, K., Moeller, L.C., Weiner, J., Heiker, J.T., et al. (2023). Thyroid hormones regulate Zfp423 expression in regionally distinct adipose depots through direct and cell-autonomous action. *Cell Rep.* 42, 112088. <https://doi.org/10.1016/j.celrep.2023.112088>.
15. Gupta, R.K., Arany, Z., Seale, P., Mepani, R.J., Ye, L., Conroe, H.M., Roby, Y.A., Kulaga, H., Reed, R.R., and Spiegelman, B.M. (2010). Transcriptional control of preadipocyte determination by Zfp423. *Nature* 464, 619–623. <https://doi.org/10.1038/nature08816>.
16. Shao, M., Ishibashi, J., Kusminski, C.M., Wang, Q.A., Hepler, C., Vishvanath, L., MacPherson, K.A., Spurgin, S.B., Sun, K., Holland, W.L., et al. (2016). Zfp423 Maintains White Adipocyte Identity through Suppression of the Beige Cell Thermogenic Gene Program. *Cell Metab.* 23, 1167–1184. <https://doi.org/10.1016/j.cmet.2016.04.023>.
17. Shao, M., Zhang, Q., Truong, A., Shan, B., Vishvanath, L., Li, L., Seale, P., and Gupta, R.K. (2021). ZFP423 controls EBF2 coactivator recruitment and PPAR γ occupancy to determine the thermogenic plasticity of adipocytes. *Genes Dev.* 35, 1461–1474. <https://doi.org/10.1101/gad.348780.121>.
18. Hepler, C., Weidemann, B.J., Waldeck, N.J., Marchecheva, B., Cedernaes, J., Thorne, A.K., Kobayashi, Y., Nozawa, R., Newman, M.V., Gao, P., et al. (2022). Time-restricted feeding mitigates obesity through adipocyte thermogenesis. *Science* 378, 276–284. <https://doi.org/10.1126/science.abl8007>.
19. Warming, S., Rachel, R.A., Jenkins, N.A., and Copeland, N.G. (2006). Zfp423 is required for normal cerebellar development. *Mol. Cell Biol.* 26, 6913–6922. <https://doi.org/10.1128/MCB.02255-05>.
20. Sassmann, A., Offermanns, S., and Wettschureck, N. (2010). Tamoxifen-inducible Cre-mediated recombination in adipocytes. *Genesis* 48, 618–625. <https://doi.org/10.1002/dvg.20665>.
21. Hesselbarth, N., Pettinelli, C., Gericke, M., Berger, C., Kunath, A., Stumvoll, M., Blüher, M., and Klötting, N. (2015). Tamoxifen affects glucose and lipid metabolism parameters, causes browning of subcutaneous adipose tissue and transient body composition changes in C57BL/6NTac mice. *Biochem. Biophys. Res. Commun.* 464, 724–729. <https://doi.org/10.1016/j.bbrc.2015.07.015>.
22. Sellers, E.A., Flattery, K.V., and Steiner, G. (1974). Cold acclimation of hypothyroid rats. *Am. J. Physiol.* 226, 290–294. <https://doi.org/10.1152/ajplegacy.1974.226.2.290>.
23. Goswami, A., and Rosenberg, I.N. (1985). Effects of thyroid status on membrane-bound low Km cyclic nucleotide phosphodiesterase activities in rat adipocytes. *J. Biol. Chem.* 260, 82–85.
24. Escobar-Morreale, H.F., del Rey, F.E., Obregón, M.J., and de Escobar, G.M. (1996). Only the combined treatment with thyroxine and triiodothyronine ensures euthyroidism in all tissues of the thyroidectomized rat. *Endocrinology* 137, 2490–2502. <https://doi.org/10.1210/endo.137.6.8641203>.
25. Trost, S.U., Swanson, E., Gloss, B., Wang-Iverson, D.B., Zhang, H., Volodarsky, T., Grover, G.J., Baxter, J.D., Chiellini, G., Scanlan, T.S., and Dillmann, W.H. (2000). The thyroid hormone receptor-beta-selective agonist GC-1 differentially affects plasma lipids and cardiac activity. *Endocrinology* 141, 3057–3064. <https://doi.org/10.1210/endo.141.9.7681>.
26. Angueira, A.R., Shapira, S.N., Ishibashi, J., Sampat, S., Sostre-Colón, J., Emmett, M.J., Titchenell, P.M., Lazar, M.A., Lim, H.-W., and Seale, P. (2020). Early B Cell Factor Activity Controls Developmental and Adaptive Thermogenic Gene Programming in Adipocytes. *Cell Rep.* 30, 2869–2878.e4. <https://doi.org/10.1016/j.celrep.2020.02.023>.
27. Dittner, C., Lindsund, E., Cannon, B., and Nedergaard, J. (2019). At thermoneutrality, acute thyroxine-induced thermogenesis and pyrexia are independent of UCP1. *Mol. Metab.* 25, 20–34. <https://doi.org/10.1016/j.molmet.2019.05.005>.
28. Nicolaisen, T.S., Klein, A.B., Dmytriyeva, O., Lund, J., Ingerslev, L.R., Fritzen, A.M., Carl, C.S., Lundsgaard, A.-M., Frost, M., Ma, T., et al. (2020). Thyroid hormone receptor α in skeletal muscle is essential for T3-mediated increase in energy expenditure. *FASEB J* 34, 15480–15491. <https://doi.org/10.1096/fj.202001258RR>.
29. Steinhoff, K.G., Krause, K., Linder, N., Rullmann, M., Volke, L., Gebhardt, C., Busse, H., Stumvoll, M., Blüher, M., Sabri, O., et al. (2021). Effects of Hyperthyroidism on Adipose Tissue Activity and Distribution in Adults. *Thyroid* 31, 519–527. <https://doi.org/10.1089/thy.2019.0806>.
30. Finan, B., Clemmensen, C., Zhu, Z., Stemmer, K., Gauthier, K., Müller, L., de Angelis, M., Moreth, K., Neff, F., Perez-Tilve, D., et al. (2016). Chemical Hybridization of Glucagon and Thyroid Hormone Optimizes Therapeutic Impact for Metabolic Disease. *Cell* 167, 843–857.e14. <https://doi.org/10.1016/j.cell.2016.09.014>.
31. Zekri, Y., Guyot, R., and Flamant, F. (2022). An Atlas of Thyroid Hormone Receptors' Target Genes in Mouse Tissues. *Int. J. Mol. Sci.* 23, 11444. <https://doi.org/10.3390/ijms231911444>.
32. Rabelo, R., Schifman, A., Rubio, A., Sheng, X., and Silva, J.E. (1995). Delineation of thyroid hormone-responsive sequences within a critical enhancer in the rat uncoupling protein gene. *Endocrinology* 136, 1003–1013. <https://doi.org/10.1210/endo.136.3.7867554>.

33. Wu, Y., Delerive, P., Chin, W.W., and Burris, T.P. (2002). Requirement of helix 1 and the AF-2 domain of the thyroid hormone receptor for coactivation by PGC-1. *J. Biol. Chem.* *277*, 8898–8905. <https://doi.org/10.1074/jbc.M110761200>.
34. Astapova, I. (2016). Role of co-regulators in metabolic and transcriptional actions of thyroid hormone. *J. Mol. Endocrinol.* *56*, 73–97. <https://doi.org/10.1530/JME-15-0246>.
35. Ribeiro, M.O., Carvalho, S.D., Schultz, J.J., Chiellini, G., Scanlan, T.S., Bianco, A.C., and Brent, G.A. (2001). Thyroid hormone–sympathetic interaction and adaptive thermogenesis are thyroid hormone receptor isoform-specific. *J. Clin. Invest.* *108*, 97–105. <https://doi.org/10.1172/JCI12584>.
36. Nedergaard, J., and Cannon, B. (2014). The browning of white adipose tissue: some burning issues. *Cell Metab.* *20*, 396–407. <https://doi.org/10.1016/j.cmet.2014.07.005>.
37. Guilherme, A., Yenilmez, B., Bedard, A.H., Henriques, F., Liu, D., Lee, A., Goldstein, L., Kelly, M., Nicoloso, S.M., Chen, M., et al. (2020). Control of Adipocyte Thermogenesis and Lipogenesis through β 3-Adrenergic and Thyroid Hormone Signal Integration. *Cell Rep.* *31*, 107598. <https://doi.org/10.1016/j.celrep.2020.107598>.
38. Rubio, A., Raasmaja, A., and Silva, J.E. (1995). Thyroid hormone and norepinephrine signaling in brown adipose tissue. II: Differential effects of thyroid hormone on beta 3-adrenergic receptors in brown and white adipose tissue. *Endocrinology* *136*, 3277–3284. <https://doi.org/10.1210/endo.136.8.7628361>.
39. Chung, G.E., Kim, D., Kim, W., Yim, J.Y., Park, M.J., Kim, Y.J., Yoon, J.-H., and Lee, H.-S. (2012). Non-alcoholic fatty liver disease across the spectrum of hypothyroidism. *J. Hepatol.* *57*, 150–156. <https://doi.org/10.1016/j.jhep.2012.02.027>.
40. Knudsen, N., Laurberg, P., Rasmussen, L.B., Bülow, I., Perrild, H., Ovesen, L., and Jørgensen, T. (2005). Small differences in thyroid function may be important for body mass index and the occurrence of obesity in the population. *J. Clin. Endocrinol. Metab.* *90*, 4019–4024. <https://doi.org/10.1210/jc.2004-2225>.
41. Sterenborg, R.B.T.M., Steinbrenner, I., Li, Y., Bujnis, M.N., Naito, T., Marouli, E., Galesloot, T.E., Babajide, O., Andreassen, L., Astrup, A., et al. (2024). Multi-trait analysis characterizes the genetics of thyroid function and identifies causal associations with clinical implications. *Nat. Commun.* *15*, 888. <https://doi.org/10.1038/s41467-024-44701-9>.
42. Harrison, S.A., Bedossa, P., Guy, C.D., Schattenberg, J.M., Loomba, R., Taub, R., Labriola, D., Moussa, S.E., Neff, G.W., Rinella, M.E., et al. (2024). A Phase 3, Randomized, Controlled Trial of Resmetirom in NASH with Liver Fibrosis. *N. Engl. J. Med.* *390*, 497–509. <https://doi.org/10.1056/NEJMoa2309000>.
43. Rahbani, J.F., Roesler, A., Hussain, M.F., Samborska, B., Dykstra, C.B., Tsai, L., Jedrychowski, M.P., Vergnes, L., Reue, K., Spiegelman, B.M., and Kazak, L. (2021). Creatine kinase B controls futile creatine cycling in thermogenic fat. *Nature* *590*, 480–485. <https://doi.org/10.1038/s41586-021-03221-y>.
44. Ikeda, K., Kang, Q., Yoneshiro, T., Camporez, J.P., Maki, H., Homma, M., Shinoda, K., Chen, Y., Lu, X., Maretich, P., et al. (2017). UCP1-independent signaling involving SERCA2b-mediated calcium cycling regulates beige fat thermogenesis and systemic glucose homeostasis. *Nat. Med.* *23*, 1454–1465. <https://doi.org/10.1038/nm.4429>.
45. Rosenwald, M., Perdikari, A., Rüllicke, T., and Wolfrum, C. (2013). Bi-directional interconversion of brite and white adipocytes. *Nat. Cell Biol.* *15*, 659–667. <https://doi.org/10.1038/ncb2740>.
46. Hönes, G.S., Rakov, H., Logan, J., Liao, X.-H., Werbenko, E., Pollard, A.S., Præsthholm, S.M., Siersbæk, M.S., Rijntjes, E., Gassen, J., et al. (2017). Noncanonical thyroid hormone signaling mediates cardiometabolic effects in vivo. *Proc. Natl. Acad. Sci.* *114*, E11323–E11332. <https://doi.org/10.1073/pnas.1706801115>.
47. Hofmann, P.J., Schomburg, L., and Köhrle, J. (2009). Interference of endocrine disrupters with thyroid hormone receptor-dependent transactivation. *Toxicol. Sci. Off. J. Soc. Toxicol.* *110*, 125–137. <https://doi.org/10.1093/toxsci/kfp086>.
48. Chen, S., Zhou, Y., Chen, Y., and Gu, J. (2018). fastp: an ultra-fast all-in-one FASTQ preprocessor. *Bioinforma. Oxf. Engl.* *34*, i884–i890. <https://doi.org/10.1093/bioinformatics/bty560>.
49. Patil, I. (2021). Visualizations with statistical details: The “ggstatsplot” approach. *J. Open Source Softw.* *6*, 3167. <https://doi.org/10.21105/joss.03167>.
50. Frankish, A., Diekhans, M., Ferreira, A.-M., Johnson, R., Jungreis, I., Loveland, J., Mudge, J.M., Sisu, C., Wright, J., Armstrong, J., et al. (2019). GENCODE reference annotation for the human and mouse genomes. *Nucleic Acids Res.* *47*, D766–D773. <https://doi.org/10.1093/nar/gky955>.
51. Ritchie, M.E., Phipson, B., Wu, D., Hu, Y., Law, C.W., Shi, W., and Smyth, G.K. (2015). limma powers differential expression analyses for RNA-seq and microarray studies. *Nucleic Acids Res.* *43*, e47. <https://doi.org/10.1093/nar/gkv007>.
52. Tingley, D., Yamamoto, T., Hirose, K., Keele, L., and Imai, K. (2014). mediation: R Package for Causal Mediation Analysis. *J. Stat. Softw.* *59*, 1–38. <https://doi.org/10.18637/jss.v059.i05>.
53. Wang, L., Nie, J., Scicotte, H., Li, Y., Eckel-Passow, J.E., Dasari, S., Vedell, P.T., Barman, P., Wang, L., Weinshiboum, R., et al. (2016). Measure transcript integrity using RNA-seq data. *BMC Bioinf.* *17*, 58. <https://doi.org/10.1186/s12859-016-0922-z>.
54. Langhardt, J., Flehmig, G., Klötting, N., Lehmann, S., Ebert, T., Kern, M., Schön, M.R., Gärtner, D., Lohmann, T., Dressler, M., et al. (2018). Effects of Weight Loss on Glutathione Peroxidase 3 Serum Concentrations and Adipose Tissue Expression in Human Obesity. *Obes. Facts* *11*, 475–490. <https://doi.org/10.1159/000494295>.
55. Mardinoglu, A., Heiker, J.T., Gärtner, D., Björnson, E., Schön, M.R., Flehmig, G., Klötting, N., Krohn, K., Fasshauer, M., Stumvoll, M., et al. (2015). Extensive weight loss reveals distinct gene expression changes in human subcutaneous and visceral adipose tissue. *Sci. Rep.* *5*, 14841. <https://doi.org/10.1038/srep14841>.
56. Picelli, S., Faridani, O.R., Björklund, A.K., Winberg, G., Sagasser, S., and Sandberg, R. (2014). Full-length RNA-seq from single cells using Smart-seq2. *Nat. Protoc.* *9*, 171–181. <https://doi.org/10.1038/nprot.2014.006>.
57. Song, Y., Milon, B., Ott, S., Zhao, X., Sadzewicz, L., Shetty, A., Boger, E.T., Tallon, L.J., Morell, R.J., Mahurkar, A., and Hertzano, R. (2018). A comparative analysis of library prep approaches for sequencing low input transcriptome samples. *BMC Genom.* *19*, 696. <https://doi.org/10.1186/s12864-018-5066-2>.
58. Robinson, M.D., and Oshlack, A. (2010). A scaling normalization method for differential expression analysis of RNA-seq data. *Genome Biol.* *11*, R25. <https://doi.org/10.1186/gb-2010-11-3-r25>.
59. Speakman, J.R., Fletcher, Q., and Vaanholt, L. (2013). The “39 steps”: an algorithm for performing statistical analysis of data on energy intake and expenditure. *Dis. Model. Mech.* *6*, 293–301. <https://doi.org/10.1242/dmm.009860>.

STAR★METHODS

KEY RESOURCES TABLE

REAGENT or RESOURCE	SOURCE	IDENTIFIER
Antibodies		
Anti-UCP1	Abcam	Cat# ab10983; RRID: AB_2241462
EnVision+ HRP labeled polymer anti-rabbit	Dako	Cat#K4003; RRID: AB_2630375
HSL	CellSignaling	Cat# 4107S; RRID: AB_2296900
IRDye 680RD goat anti-mouse	LI-COR	Cat# 926-68070; RRID: AB_10956588
IRDye 800CW goat anti-rabbit	LI-COR	Cat# 926-32211; RRID: AB_621843
Phospho-HSL (Ser660)	CellSignaling	Cat# 45804S; RRID: AB_2893315
Chemicals, peptides, and recombinant proteins		
Albumin Fraction V	Roth	Cat# 8076.2
Ascorbic Acid	Sigma Aldrich	Cat# A92902
BCA Protein Assay Kit	ThermoFisher Scientific	Cat# 23225
cOmplete protease inhibitor cocktail	Roche	Cat# 11697498001
Dexamethasone	Sigma Aldrich	Cat# D-4902
DMEM	Gibco	Cat# 41966
FBS (Fetal bovine serum) superior	Sigma Aldrich	Cat# S0615
Forskolin	Sigma Aldrich	Cat# F3917
Fugene HD	Promega	Cat# E2311
GC-1 (Sobetirome)	Tocris	Cat# 4554
4-hydroxytamoxifen	Sigma Aldrich	Cat# H6278
IBMX (3-Isobutyl-1-methylxanthin)	Sigma Aldrich	Cat# I-5879
Insulin	Roche	Cat# 1376497
Norepinephrine-bitartrate	Sigma Aldrich	Cat# A0937
PhosSTOP phosphatase inhibitor cocktail	Roche	Cat# 4906837001
Rosiglitazone	Sigma Aldrich	Cat# R2408
Sinora norepinephrine	Sintetica	PZN12474594
T3 (3,3',5-Triiodo-L-Thyronine)	Sigma Aldrich	Cat# T6397
T4 (L-Thyroxin)	Sigma Aldrich	Cat# T2376
Tamoxifen	Sigma Aldrich	Cat# T5648
ZellShield	Minerva Biolabs	Cat# 13-0050
Critical commercial assays		
cAMP Assay Kit (competitive ELISA, fluorometric)	abcam	Cat# ab138880
Dual-Glo Luciferase Assay System	Promega	Cat# E2920
Free T3 ELISA	DRG Diagnostics	Cat# EIA-3801
LightCycler 480 SYBR Green I Master	Roche	Cat# 4887352001
Nextera DNA Flex Library Prep Kit	Illumina	Cat# 20018705
Revert 700 total protein stain kit	LI-COR	Cat# 926-11010
RNeasy Lipid Tissue Mini Kit	Qiagen	Cat# 74104
Seahorse XF DMEM assay medium pack	Agilent	Cat# 103680-100
Seahorse XF Cell Mito Stress Test Kit	Agilent	Cat# 103015-100
Total T4 ELISA	DRG Diagnostics	Cat# EIA-4568

(Continued on next page)

Continued		
REAGENT or RESOURCE	SOURCE	IDENTIFIER
Experimental models: cell lines		
Murine: 3T3-L1 cells	ATCC	Cat# CL-173 RRID: CVCL_0123
Experimental models: organisms/strains		
Mouse: C57BL/6NTac	Taconic Europe	RRID: IMSR_TAC:b6
Mouse: C57BL/6-Tg(Adipoq-icre/ERT2)1Soff/J	Jackson Laboratory, Sassmann et al. ²⁰	RRID: IMSR_JAX:025124
Mouse: Tg(Ucp1-cre/ERT2)426Biat	Rosenwald et al. ⁴⁵	N/A
Mouse: Zfp423(tm1.1Ngc)	Genentech, Warming et al. ¹⁹	RRID: MGI 3653604
Oligonucleotides		
Primers for qPCR (see Table S4)	This Paper	N/A
Recombinant DNA		
pcDNA3.1_EBF2	GenScript	Cat# NM_001276387.1
pcDNA3.1_PGC1a	GenScript	Cat# NM_008904.2
pcDNA3.1_TRa	Hönes et al. ⁴⁶	N/A
pcDNA3.1_TRb	Hönes et al. ⁴⁶	N/A
pcDNA3.1_Zfp423	Gupta et al. ¹⁵	N/A
p(DR4)2-SV40-luc+	Hofmann et al. ⁴⁷	N/A
pGL4.23[luc2/minP]	Promega	Cat# E8411
pGL4.74[hRluc/TK]	Promega	Cat# E6921
Software and algorithms		
corrplot	N/A	https://cran.r-project.org/web/packages/corrplot/index.html
ezRun (v3.14.1)	N/A	https://github.com/uzh/ezRun
Fastp (v0.20.0)	Chen et al. ⁴⁸	https://github.com/OpenGene/fastp
ggpubr (v.0.4.0)	N/A	https://cran.r-project.org/web/packages/ggpubr/index.html
GraphPad Prism (v10.0)	GraphPad	https://www.graphpad.com/
ggstatsplot (v0.9.1)	Patil et al. ⁴⁹	https://cran.r-project.org/web/packages/ggstatsplot/index.html
kallisto (v 0.48)	Frankish et al. ⁵⁰	https://github.com/pachterlab/kallisto
limma (v3.56.2)	Ritchie et al. ⁵¹	https://bioconductor.org/packages/release/bioc/html/limma.html
mediation (v4.5.0)	Tingley et al. ⁵²	https://cran.r-project.org/web/packages/mediation/index.html
R (v4.3.1)	R Core Team	https://cran.r-project.org/bin/windows/
RSeQC (v4.0.0)	Wang et al. ⁵³	https://github.com/MonashBioinformaticsPlatform/RSeQC
Other		
iodine-free chow diet supplemented with 0.15% propylthiouracil	Ssniff	Cat# E15551
Control chow diet	Ssniff	Cat# E15552-24

EXPERIMENTAL MODEL AND STUDY PARTICIPANT DETAILS

Human cohort

The Leipzig Obesity BioBank (LOBB) has established a cross-sectional cohort of 1,202 individuals, encompassing various biomaterials such as serum, plasma, visceral (VAT) and subcutaneous (SAT) adipose tissue. Among the participants are 1,176 obese individuals (77% women, age = 46.7 ± 11.7 years, BMI = 49.3 ± 8.4 kg/m²; glucose metabolism characteristics: *N* = 604 with normal glucose tolerance (NGT), *N* = 27 with impaired fasting glucose (IFG), *N* = 42 with impaired glucose tolerance (IGT), *N* = 502 with type 2 diabetes (T2D)) and 26 non-obese patients (46% women, age = 54.9 ± 14 years, BMI = 25.4 ± 2.8 kg/m²; glucose metabolism characteristics:

$N = 24$ with NGT, $N = 2$ with T2D). The collection of VAT and SAT samples occurred during elective laparoscopic abdominal surgery from 2008 to 2018, as previously documented.^{54,55} Exclusion criteria comprised individuals under the age of 18, chronic substance or alcohol misuse, smoking, acute inflammatory diseases, use of glitazones as concomitant medication, end-stage malignant diseases, uncontrolled thyroid disorder, L-Thyroxin intake and Cushing's disease. The study was performed in agreement with the Declaration of Helsinki and approved by the Ethics Committee of the University of Leipzig (approval number: 159-12-21052012). All participants gave written informed consent before taking part in the study.

Animals

All animal experiments were performed according to guidelines approved by local authorities of the State of Saxony, Germany as recommended by the responsible local animal ethics review board (Regierungspräsidium Leipzig, TVV10/18, TVV41/21, Germany). Mice were randomly allocated to experimental groups after checking that initial body weights were not statistically different. Mice were maintained in groups of five on a 12:12-h dark-light cycle with free access to water and food.

The Zfp423^{loxP/loxP} mouse line was generously provided by Dr. S. Warming (Genetech) and was previously described.¹⁹ The *Adipoq*_CreER^{T2} line was obtained from Jackson Laboratory²⁰ and Tg(Ucp1-cre/ERT2)426Biat line was obtained from Prof. Dr. Wolf-rum.⁴⁵ The Zfp423iAKO line was generated by breeding Zfp423^{loxP/loxP} mouse with *Adipoq*_CreER^{T2} mouse.²⁰ Zfp423iBATKO mice were created by breeding Zfp423^{loxP/loxP} with Tg(Ucp1-cre/ERT2)426Biat mice. Littermates carrying Zfp423-*loxP/loxP* alleles and negative for CreERT allele served as control.

At the age of 8 weeks, female Zfp423iAKO and Zfp423iBATKO mice were rendered hypothyroid or euthyroid by feeding an iodine-free chow diet supplemented with 0.15% propylthiouracil (PTU) for 4 weeks or a control chow diet, respectively (ssniff, Germany). Adipocyte-specific Zfp423 knockout was induced at the age of 10 weeks by treatment with tamoxifen (1 mg, i.p. for 5 days, Sigma Aldrich, USA). After 10 days of washout, mice were characterized by indirect calorimetry and infrared thermography and were dissected.

For temperature experiments, Zfp423iAKO mice were maintained in a temperature-controlled climate chamber (HPP750, Memmert, Germany) at 30°C, 22°C or 18°C during the 4 weeks of treatment. Acute NE injection (1 µg/g body weight, s.c., Sintetica, Switzerland) was carried out at the end of treatment after repeated training injections with saline to minimize stress induced response. For GC-1 treatment, hypothyroid Zfp423iAKO mice were injected with GC-1 (Tocris, UK) in a low dose (1.8 ng/g body weight, i.p., 10 days) or a higher, supraphysiological dose (300 ng/g body weight, i.p., 14 days) during the last days of PTU treatment.

Primary cell culture

Stromal vascular fraction (SVF) of 8–12 week-old female mice were isolated and differentiated as follows: iWAT depot was minced and digested in HEPES isolation buffer (100 mM HEPES, 123 mM NaCl, 5 mM KCl, 1.3 mM CaCl₂, 5 mM glucose, 4% BSA, 1% ZellShield, 0.2% (w/v) collagenase II, pH 7.2) at 37°C for 45 min. The suspension was filtered through a 100 µm cell strainer, subsequently placed on ice for 15 min to separate SVF from mature adipocytes and filtered through a 40 µm cell strainer. Erythrocytes were lysed with erythrocyte lysis buffer for 5 min. Cells were seeded in DMEM (Gibco, USA) supplemented with 10% FBS, 25 µg/mL ascorbic acid and 1% ZellShield. Medium was changed the first day and then every second day. Primary cells were cultured at 37°C and 5% CO₂.

Cell lines

3T3-L1 cells were purchased from ATCC (#CL-173, Mus Musculus, male) and were tested negative for mycoplasma contamination (MycoAlert™ PLUS Mycoplasma Detection Kit, Lonza). Cells were cultured at 37°C and 5% CO₂.

METHOD DETAILS

Bulk RNA sequencing and analysis of human data

The RNA-seq data was generated using the SMARTseq protocol, involving single-end sequencing and rRNA depletion.^{56,57} Initially, RNA was enriched, and reverse transcribed using Oligo(dT) and TSO primers. ISPCR primers were utilized for cDNA amplification, followed by processing with Tn5 using the Nextera DNA Flex kit. Subsequently, all libraries were sequenced on a Novaseq 6000 instrument at the Functional Genomics Center Zurich (FGCZ). Raw sequencing reads were preprocessed using Fastp (v0.20.0),⁴⁸ then aligned against the human reference genome (assembly GRCh38.p13, GENCODE release 32) and gene-level expression quantified using Kallisto (v 0.48).⁵⁰ In cases of excessive read counts, samples were down-sampled to 20 million reads using the R package ezRun (v3.14.1; <https://github.com/uzh/ezRun>, accessed on 23 March 2022). The data was normalized using the trimmed mean of M-values (TMM) method and subsequently log-transformed.⁵⁸ Batch effects were assessed and adjusted using limma (v3.56.2).⁵¹ The data was adjusted for age, gender, and transcript integrity numbers (TIN), which were calculated using the R package RSeQC v4.0.0.⁵³

Metabolic phenotyping of mice

Body weight and rectal body temperature was measured three times a week. Energy expenditure was measured by indirect calorimetry using CaloSys V2.1 metabolic chamber (TSE Systems, Germany). After one day of acclimatization, data was recorded every

5 min over a time period of 48 h. To measure NE-stimulated energy expenditure, data was recorded every minute. After one day of acclimatization, basal metabolic rate was measured for 1 h, mice were injected with NE and metabolic rate was measured for another 3 h until values stabilized to the basal level.

Infrared thermography

At the end of treatment, BAT and tail surface temperature were measured by thermal imaging using the VarioCAM hr system (Infratec, Germany). During imaging, the mice moved freely on the floor of a cage. BAT temperature was determined between the shoulder blades and tail temperature was determined 0.5 cm from the tail root. Three images per mouse were averaged.

ELISA

Thyroid status of mice was validated with commercially available tT4 and fT3 ELISA kits according to the manufacturer's instructions (DRG diagnostics, Germany). For cAMP detection, 15–20 mg of iWAT were homogenized with 12.5 $\mu\text{L}/\text{mg}$ Cell Lysis Buffer of cAMP Assay Kit (abcam, UK) and samples were measured according to the manufacturer's instructions.

Western Blot analysis

Proteins from adipose tissues were extracted with RIPA buffer (150mM NaCl, 10mM Tris (pH 7.2), 0.1% SDS, 1% TX100, 1% deoxycholate, 5mM EDTA), supplemented with protease and phosphatase inhibitor cocktail (Roche, Switzerland), and quantified using BCA Protein Assay Kit (ThermoFisher Scientific, USA). 30 μg of protein lysates were subjected to SDS-PAGE and transferred to nitrocellulose membranes by tank blot. Total protein was quantified with Revert 700 total protein stain kit (LI-COR, USA). Membranes were incubated with the following primary antibodies: UCP1 (abcam, UK), pHSL (CellSignaling, UK), HSL (CellSignaling, UK). After incubation with secondary antibodies (IRDye 800CW goat anti-rabbit, IRDye 680RD goat anti-mouse, LI-COR, USA), fluorescence intensity was detected using Odyssey XF Imager (LI-COR, USA). For calculation of UCP1 protein amount per depot, UCP1 signal per μg was multiplied by the protein density of the RIPA lysate [μg per mg tissue] and the measured tissue weight [mg].

Immunohistochemistry

After fixation in 4% formaldehyde for 24 h at 4°C, iWAT and gWAT samples were embedded in paraffin and cut into 5 μm sections. Staining was done using the primary antibody UCP1 (abcam, UK) and HRP-conjugated anti-rabbit antibody (Dako Envision, Dako, Germany). Pictures were taken with BZ-X800 microscope (Keyence, Japan).

Oxygen consumption assay in primary adipocytes

After reaching confluence, SVF cells derived from iWAT of *Zfp423iAKO* and control mice were incubated with differentiation medium (culture medium supplemented with 100 nM insulin, 1 μM rosiglitazone, 0.4 $\mu\text{g}/\text{mL}$ dexamethasone, 250 μM IBMX) for 48 h, followed by culture medium with 100 nM insulin for 48 h. Subsequently, cells were incubated with culture medium supplemented with 1 μM 4-hydroxytamoxifen for 48 h to induce *Zfp423* knockout. Cells were detached with 0.02% collagenase II in 0.25% trypsin/EDTA solution and seeded into gelatin-coated 96-well Seahorse assay plates at a density of 2×10^4 cells per well. After 48 to 72 h, cells were washed two times with assay medium (Seahorse XF DMEM, pH 7.4, supplemented with 10 mM glucose, 2 mM L-glutamine and 1 mM pyruvate) and incubated in assay medium for 45 min at 37°C without CO₂. Oxygen consumption rate (OCR) was measured in SeahorseXFe96 analyzer after injection of 2 μM oligomycin (Oli), 2.5 μM FCCP and 0.5 μM rotenone/antimycin A (Rot/AA) (Mito Stress Test, Agilent, USA). OCR was analyzed (I) after incubation with 1 μM NE (Sigma Aldrich, USA) the last 24 h before measurement (II) upon acute stimulation with 5 μM NE or 5 μM forskolin (FKS) and (III) after pre-incubation with 200 μM IBMX for 45 min. The different components of mitochondrial respiration were calculated as follows: Basal respiration = [basal OCR] – [minimal OCR (Rot/AA)]; ATP-coupled respiration = [basal OCR] – [minimal OCR (Oli)]; uncoupled respiration = [minimal OCR (Oli)] – [minimal OCR (Rot/AA)]; uncoupling response = [maximal OCR (NE/FSK)] – [minimal OCR (Oli)]; maximal respiration = [maximal OCR (FCCP)] – [minimal OCR (Rot/AA)]. During adipogenic differentiation and treatment, TH-depleted FBS (produced as described by Samuels et al.) was used and supplemented with 10 nM T3 or solvent (40 mM NaOH) to mimic euthyroid or hypothyroid conditions, respectively. For each experimental group, iWAT of $n = 3$ mice was pooled and at least $n = 6$ replicates from independent wells were measured.

Gene expression analysis

Total RNA from tissue or cell culture was extracted with the RNeasy Lipid Tissue Mini Kit (Qiagen, Netherlands). Complementary DNA was synthesized using random hexamer primers and M-MLV reverse transcriptase (Promega, USA). Quantitative real-time PCR was performed with LightCycler System LC480 using LightCycler-DNA Master SYBR Green I Kit (Roche, Germany) and gene expression was calculated by delta-delta CT method with *Rplp0* as reference gene. Primer sequences are provided in Table S4.

Luciferase gene reporter assay

Ucp1_6kb enhancer²⁶ was cloned into pGL4.23 firefly luciferase reporter plasmid (Promega, USA). 3T3-L1 cells were seeded in 24-well plates at a density of 1.5×10^4 cells per well in DMEM containing 10% FBS. After 24 h, cells were transfected with 250 ng of pGL4.23-enhancer plasmid using FUGENE HD (Promega, USA). Cells were co-transfected with 25 ng of indicated expression plasmids (pcDNA, pcDNA_EBF2, pcDNA_PGC1a, pcDNA_TRa, pcDNA_TRb, pcDNA_Zfp423) and 5 ng of pGL4.74 (renilla) as

internal control. Medium was replaced with DMEM containing 10% TH-depleted FBS after 6 h. One day after transfection, cells were treated with 10 nM T3 or solvent (40 mM NaOH) for 24 h. Cells were harvested in passive lysis buffer and firefly luciferase activity was determined and normalized to renilla luciferase activity using the Dual-Luciferase Reporter Assay System (Promega, USA). Functionality of TH signaling was evaluated with p(DR4)2-SV40-luc+ plasmid⁴⁷ that was provided by L. Schomburg, University of Berlin. Assay was run in duplicates and was repeated three times.

QUANTIFICATION AND STATISTICAL ANALYSIS

Human RNA-seq data was analyzed in R v4.3.1. Gene expression between SAT and VAT was compared with Mann-Whitney U test and Dunn's post-hoc test for pairwise multiple comparison with Holm p -value adjustment using the R package ggstatsplot⁴⁹ and was plotted with ggpubr. Correlations were calculated based on Spearman correlation coefficient and a confidence interval of 0.95 using the R packages ggpubr and corplot. Causal mediation analysis based on nonparametric bootstrap confidence intervals was constructed by the percentile method and 1000 resamples using R package mediation.⁵² Animal data and *in vitro* experiments were analyzed with GraphPad Prism 10.0 software (GraphPad, USA) using two-way ANOVA with Tukey post-hoc test for multiple comparison. The minimum of animals allowing statistical significance has been calculated and accepted by the ethical committee based on previous studies in the same field. Indirect calorimetry data was analyzed in R v4.3.2 as previously described.⁵⁹ Shortly, the effects of genotype, TH level, treatment and temperature as well as genotype interactions were calculated with two-way ANOVA and Tukey post-hoc test, followed by ANCOVA analysis to confirm independence from the covariate body weight. Statistical information, sample sizes, replications and p -values are provided in the figure legends. N values represent biological replicates unless otherwise stated.